NUMERICAL SIMULATION OF FLOW AND HEAT TRANSFER AROUND AN OCTAGONAL BLUFF BODY

THESIS SUBMITTED IN PARTIAL FULFILMENTS OF THE REQUIREMENT FOR THE DEGREE OF MASTER OF ENGINEERING IN MECHANICAL ENGINEERING UNDER FACULTY OF ENGINEERING AND TECHNOLOGY

Submitted by

BABLU KUMAR SAW

Class Roll Number: 002111202019

Registration No.:160285 of 2021-2022

Exam Roll No.: M4MEC23010

Academic Session: 2021-2023

Under the guidance of

Prof. Sudhir Chandra Murmu

Department of Mechanical Engineering,
Jadavpur University

DEPARTMENT OF MECHANICAL ENGINEERING
JADAVPUR UNIVERSITY

DECLARATION OF ORIGINALITY AND COMPLIANCE OF ACADEMIC ETHICS

I hereby declare that the thesis entitled "**NUMERICAL SIMULATION OF FLOW AND HEAT TRANSFER AROUND AN OCTAGONAL BLUFF BODY**" contains literature survey and original research work by the undersigned candidate, as a part of his *MASTER OF ENGINEERING IN MECHANICAL ENGINEERING under the DEPARTMENT OF MECHANICAL ENGINNERING,* studies during academic session 2021-2023.

All information in this document have been obtained and presented in accordance with the academic rules and ethical conduct.

I also declare that, as required by these rules of conduct, I have fully cited and referenced all the material and results that are not original to this work.

Name: **BABLU KUMAR SAW**

Class Roll Number: **002111202019**

University Registration No: 160285 of 2021-2022

Examination Roll No: M4MEC23010

Date:

Signature:

FACULTY OF ENGINEERING & TECHNOLOGY

DEPARTMENT OF MECHANICAL ENGINEERING
JADAVPUR UNIVERSITY
KOLKATA

CERTIFICATE OF RECOMMENDATION

This is to certify that the thesis entitled " **NUMERICAL SIMULATION OF FLOW AND HEAT TRANSFER AROUND AN OCTAGONAL BLUFF BODY**" is a bonafide work carried out by BABLU KUMAR SAW under our supervision and guidance in partial fulfilment of the requirements for awarding the degree of Master of Engineering in Mechanical Engineering under Department of Mechanical Engineering, Jadavpur University during the academic session 2021-2023.

THESIS SUPERVISOR
Prof. Sudhir Chandra Murmu
Department of Mechanical Engineering
Jadavpur University, Kolkata

Prof. Amit Karmakar
Head of the Department
Department of Mechanical Engineering
Jadavpur University, Kolkata

Prof. Saswati Mazumdar
Dean
Faculty Council of Engineering & Technology
Jadavpur University, Kolkata

FACULTY OF ENGINEERING & TECHNOLOGY
DEPARTMENT OF MECHANICAL ENGINEERING
JADAVPUR UNIVERSITY
KOLKATA-700032

CERTIFICATE OF APPROVAL

The foregoing thesis, entitled "**NUMERICAL SIMULATION OF FLOW AND HEAT TRANSFER AROUND AN OCTAGONAL BLUFF BODY**" is hereby approved as a creditable study in the area of Heat Power Engineering carried out and presented by BABLU KUMAR SAW in a satisfactory manner to warrant its acceptance as a prerequisite to the degree for which it has been submitted. It is notified to be understood that by this approval, the undersigned do not necessarily endorse or approve any statement made, opinion expressed and conclusion drawn therein but approve the thesis only for the purpose for which it has been submitted.

Committee of final evaluation of thesis:

Signature of Examiners

ACKNOWLEDGEMENT

I would like to record here my gratitude to all who supported me and gave constructive suggestions during the completion of this paper.

Separately, I express my deepest gratitude to **Prof. Sudhir Chandra Murmu**, Department of Mechanical Engineering. The regular discussions and idea-sharing with my thesis supervisors really helped me to improve my knowledge day by day my research related problems. At the beginning of this work, they gave me the valuable instruction that properly guided me in right path to accomplish this paper. It was really a pleasure work under their supervision.

I sincerely believe that I was fortunate enough to have come across **Prof. Sudhir Chandra Murmu**, who can inspire someone to work wonders. It would really have been not possible for me to complete this thesis without his assistance, proper guidance and motivation. He always helped me during the critical phase of this thesis and was always available for me for any query, whether it's a telephonic or a face to face discussion. Above all he enhanced my confidence and guided me throughout my work.

I firmly believe that I was fortunate to have met **Prof. Himadri Chattopadhyay**, Department of Mechanical Engineering, Jadavpur University, who has the ability to motivate people to do great things. Without his aid, the right direction, and the determination to finish this thesis, it would not have been feasible for me to do so. He always supported me as I worked through the revision process for this thesis and was always there to answer any questions I had. Above all, he boosted my confidence and helped me get the job done.

I also tender my sincere gratitude to **Mr. Saumendra Nath Mishra,** PhD scholar, whose continuous guidance helped me a lot in carrying out a major portion of my work. Without his wise and valuable advices, it would not be possible to prepare such a thesis.

I would like to thank **Mr. Sudipta Saha**, PhD scholar, for giving me valuable suggestions and the instant ideas which played an important part to process the thesis.

I also like to thank **Mr. Satyajit Biswas**, PhD Scholar, for implying his knowledge in the Ansys Software for doing geometry, meshig work and his assistance in my work.

I would like to thank **Mr. Joy Mandal** and **Mr. Manish Kumar Manna**, PhD scholar, Department of Mechanical Engineering, for their instant help and providing ideas.

I am highly indebted to all my seniors of **NEPTUNE** lab, their guidance and supervision as well as for providing necessary information regarding thesis and also for their support in completing my master's thesis.

I would like to express my gratitude towards my parents and my younger brother for their kind cooperation and encouragement which helped me in the completion of my master's thesis.

Finally, my thanks and appreciations also go to my dear friends in developing my master's project and people who have willingly helped me out with their abilities.

BABLU KUMAR SAW

M.E ("Mechanical Engineering")

2nd Year, Final Semester

Department of Mechanical Engineering

Jadavpur University, Kolkata

TABLE OF CONTENTS

NOMENCLATURE

A : Area (m^2)

a : Transitional model constant

C_d : Drag co-efficient

C_f : Skin friction coefficient

C_p : Pressure co-efficient

H : Height of the computational domain (m)

D : Side of the bluff body (m)

h : Heat transfer coefficient (w/m^2K)

h_d : Hydraulic diameter

E : Model destruction terms

F_1, F_2: Blending function in SST model

k : Thermal conductivity

L : Length of computational domain

Nu : Nusselt number

N_{avg} : Average Nusselt number

p : Pressure (Pa)

P : Model production term

Pr : Prandtl number

Re : Reynolds number based on hydraulic diameter of bluff body

S : Absolute value of the shear strain (s^{-1})

TI : Turbulent intensity

T_s : Bluff body wall temperature (K)

T_∞ : Free stream temperature (K)

U_∞ : Free stream velocity (m/s)

X_i : Tensor co-ordinate direction

x,y,z : Cartesian co-ordinates

β_1, β_2: SST model constants

μ : Dynamic viscosity (kg/m-s)

κ : Turbulent kinetic energy (m^2/s^2)

ν : Kinematic viscosity (m^2/s)

σ : Prandtl-like diffusivities

γ : Intermittency

ω : Specific rate of turbulence dissipation (s^{-1})

Π : Intermittency adjunct function

ρ : Density (kg/m^3)

Θ : Dimensionless temperature

τ : Wall shear stress (N/m^2)

avg : Average

Eff : Effective property

i,j : Tensior notations

turb : Turbulent

List of Figures

ABSTRACT

Flow around bluff bodies have received attention of researchers over the years . In this work, transport phenomena around a octagonal bluff body has been numerically investigated.Heat transfer characterstics inside a channel in presence of bluff body and effect of turbulent intensity on transport process around a bluff body encompassing laminar and turbulent regime covering a Reynolds number range of 100 to 100,000 along with turbulent intensities varying from 5% to 40% are studied in this work. This work demonstrates that SST models can effortlessly bridge all flow regimes for predicting the heat transfer. It also quantifies the effect of inlet turbulence intensity on enhancing heat transfer from the cylinder.

While transport phenomena in external flows over bluff bodies have been studied thoroughly, comparetively few works report flow and heat transfer studies over octagonal bluff bodies. The flow field around a bluff body and associated heat transfer are nevertheless important for design of power plant machineries. This work comprises of two parts. A geometry of bluff body has been designed and then, simulation is performed over the octagonal bluff body which includes laminar and turbulent regime in the Reynolds number ranges from 100–100,000.The governing equation has been solved are continuity, momentum and energy equations.

Recent research (e.g. Abraham et al., 2009) has demonstrated that the transition SSST model developed by Menter et al. (2002) is able of properly connecting the laminar and turbulent regimes in the transition zone. Here, the turbulent viscosity is calculated to take the changing flow field into account. The addition of an intermittency parameter creates a divergence from the traditional two-equation model. This variable has a range of 0 to 1.0. The computation indicates a zero value of intermittency for a pure laminar regime.

The Reynolds number in this work is based on the shape of the bluff body. It is assumed that the bluff body's surface temperature will always be lower than the temperature of the incoming fluid stream. There have also been computed for the steady and transient versions of the SST model in addition to laminar computing in the low Re region.

Chapter 1

INTRODUCTION

Numerous researchers have thoroughly investigated the flow around a bluff body in ducts and channels using both numerical and experimental techniques. In-depth studies have been conducted over the years on the flow of fluid and the transfer of heat past bluff bodies with various cross section geometries. For circular, square, and rectangular-shaped bodies, the majority of the work is devoted to comprehending the complex stream physics and thermo-fluid transport phenomenon. External flow and internal flow are two different types of flows that depend on whether the fluid is moving over the surface or inside the conduit. Internal flow frequently exhibits a very different characteristic from flow. A bluff body (i.e. external flow) is one in which the length in the flow direction is close or equal to the length perpendicular to the flow direction. A body is also known as a bluff and a in other contexts is associated with a significant pressure drag. In nuclear power plants, the Reynolds number typically has a high value for heating and cooling systems. Although recently there has been a lot of emphasis on lines, offshore structures, buildings, chimneys, stints, grids, screens, and cables, Re can be relatively low in these structures. A number of important physical phenomena, such as flow separation, vortex shedding, and the change from laminar to turbulent flow, are particularly evident in the flow around octagonal bluff body. The shape of a body determines how energy transforms, moves through, and moves through it.

Numerical simulation is a key tool for understanding and analyzing heat transfer and fluid flow phenomena around various geometries. An "octagonal bluff body" is a solid with an eight-sided polygonal cross-section, which serves as an example of this geometry. Bluff bodies are used in a variety of engineering applications, including the construction of buildings, vehicles, and commercial equipment. In order to enhance the design, functionality, and operational safety of such bodies, it is crucial to understand the characteristics of heat transfer around them. The fundamental process of heat transfer is used and involved in numerous natural and artificial systems. A temperature gradient causes thermal energy to be transferred from one area or material to another. The analysis of heat transfer in bluff bodies exposed to fluid flows, such as air or water currents, is particularly important in this situation. Numerical simulations are a quick and efficient way to examine the behavior of heat transfer around bluff bodies. Using computational fluid dynamics (CFD) methods, researchers can model and examine the complex fluid flow patterns and temperature distribution around the octagonal bluff body under various conditions. Fluid velocity, temperature gradients, and the geometrical features of the bluff body will all be factors in the investigation. The outcomes of the simulations will be used to comprehend the mechanisms of heat transfer and to identify the factors that have an impact on how well heat is removed from the surface of the bluff body. The potential of this study to enhance the heat transfer effectiveness of bluff body designs and to direct engineering practices in a variety of industries makes it significant. A thorough knowledge of heat transfer around

bluff bodies can also aid in the design of heat exchangers, buildings, and other engineering structures that are subject to fluid flow, as well as enhance thermal management methods and energy conservation. The primary focus of this study is on the numerical simulation of heat transfer around an octagonal bluff body. Understanding the heat transfer behavior around such bluff bodies is crucial for a variety of engineering applications, including aerodynamics, architecture, and industrial processes. To achieve this, computational fluid dynamics (CFD) techniques will be used to simulate the flow field and temperature distribution around the bluff body. The numerical simulations will also provide in-depth information about vortices, flow separation, and recirculation zones, all of which have a significant impact on heat transfer around the bluff body. The findings of this investigation will contribute to a fundamental understanding of the heat transfer phenomena around octagonal bluff bodies and will have direct applications in the design and optimization of various engineering systems. Understanding the fluid dynamics and heat transfer around bluff bodies allows engineers and scientists to develop more efficient and environmentally friendly technologies for a variety of applications. Through this study, we aim to provide in-depth knowledge into the complex heat transfer behavior around octagonal bluff bodies, contributing to the fields of fluid dynamics and heat transfer.

a) Bluff bodies

Bluff bodies are impediments or items that are placed in the way of a fluid flow in fluid dynamics and cause the flow pattern to be disrupted. Due to the distinctive shape of these bodies, the flow separates around them, causing turbulence and pressure differences. In several engineering fields, including as aerodynamics, civil engineering, and automobile design, bluff bodies are crucial. Bland bodies are frequently seen as cylinders, spheres, cubes, and airfoils. They are frequently employed in computational fluid dynamics (CFD) simulations and wind tunnel testing to investigate the flow behavior and aerodynamic properties of various shapes. The creation of a wake behind bluff bodies is one of their key characteristics. The area of disrupted flow immediately downstream of the object is known as the wake. This wake may be advantageous in some circumstances, such as when providing down force for race cars or lift for flying objects. In other circumstances, though, it could result in undesired drag and have an impact on how well a structure or item performs in general. In order to improve designs, decrease drag, increase lift, and increase overall efficiency in a variety of applications, from automobiles and aircraft to buildings and bridges, scientists and engineers analyze the behavior of bluff bodies. Engineering best practices must take into account the intricate flow patterns that surround these bodies.

b) Aerodynamic body

When moving through a fluid medium like air or water, such as, an aerodynamic body is a shape or design that is optimized to reduce drag and increase efficiency. Aerodynamic drag reduction is a crucial concept in the fields of aviation, automotive engineering, and sports because it can improve performance, fuel efficiency, and speed.

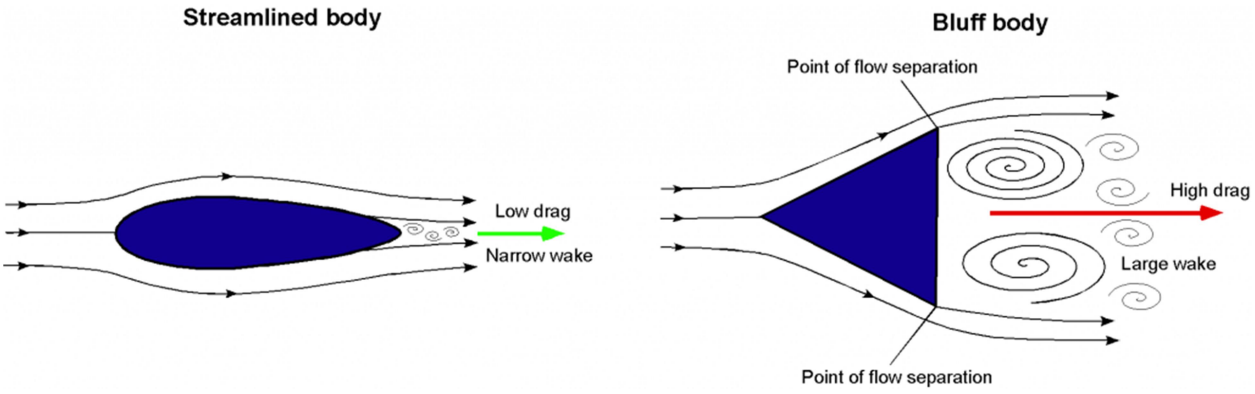

Fig. 1: (a) Streamlined Body (b) Bluff Body

Streamlined body: A body that has been streamlined is shaped to travel through a fluid more effectively by reducing drag and resistance. These bodies often have gently curved surfaces that aid in guiding the fluid smoothly around the object, as well as a smooth and aerodynamically effective profile. In applications where lowering drag is crucial, such as in aircraft, high-speed trains, and streamlined vehicles like racing cars, streamlined bodies are frequently utilized.

Bluff body: A bluff body, on the other hand, is a shape that is not streamlined and has a sizable cross-sectional area that is perpendicular to the flow direction. Due to the splitting of flow and development of a considerable turbulent wake behind them, bluff bodies significantly increase the resistance or drag they experience when moving through a fluid.

c) Types of bluff bodies

Octagonal bluff body: An octagonal bluff body is a specific geometric shape in the fields of fluid mechanics and aerodynamics. Bluff bodies are objects that, in the study of fluid dynamics, cause flow separation and turbulence as fluid flows around them.

Circular bluff body: A circular bluff body is a particular type of object or structure with a bluff shape that interacts with fluid flow, such as air or water, and causes aerodynamic or hydrodynamic effects.

Square bluff body: It is a physical entity or category of flow obstruction that is used in fluid dynamics and aerodynamics experiments.

Triangular bluff body: A triangular bluff body is a type of aerodynamic or hydrodynamic structure that has a triangular cross-section and is used to study the flow of fluid or air around it. It is frequently used in fluid dynamics experiments and wind tunnel testing to understand the behavior of flow patterns and forces acting on the body.

Rhombus bluff body: A rhombus is a four-sided polygon with equal-length sides, but unlike a square, the angles aren't always 90 degrees. This shape, when used as a bluff body, can have interesting flow characteristics because of its asymmetrical nature.

Rectangular bluff body: When studying the flow of fluids, like air or water, around an object, such as a rectangular bluff body, fluid dynamics and aerodynamics are used. Bluff bodies are described as having a noticeable width or thickness in relation to the flow direction. They are known as "bluff" because they obstruct the flow and cause turbulence, in contrast to streamlined bodies, which have smoother shapes to reduce resistance.

Semi-circular bluff body: A particular shape of an object or structure in the discipline of fluid dynamics and aerodynamics is known as a semi-circular bluff body. When exposed to a fluid stream, such as air or water, a "bluff body" is usually seen as an object or structure that significantly divides the flow and causes drag.

d) Application of bluff bodies

1. Aerodynamics and wind engineering: In the investigation of the flow of fluids around different forms, including structures, bridges, and vehicles (e. It is necessary to comprehend aerodynamic forces and flow patterns in order to design safe and reliable structures.

2. Bluff bodies are used in heat exchangers and cooling systems to improve the effectiveness of heat transfer. The flow separation and turbulence produced by bluff bodies enhance the heat transfer rates between the fluid and the solid surface.

3. Bluff bodies allow for the manipulation and control of fluid flow.

4. In sports like cycling and racing, bluff bodies are used to optimize the design of sports equipment like helmets and bicycles. By taking aerodynamics into consideration, engineers can reduce drag and improve performance.

5. Environmental Monitoring: In anemometers and wind vanes, which are used to measure wind speed and direction, bluff bodies are used to measure air quality.

6. Bluff bodies are used in fluid structure interaction (FSI) studies to examine how structures interact with the fluid they are in. Understanding how wind and water affect various structures, including offshore platforms, bridges, and towers, are essential.

7. Pollution Control: Bluff bodies are used in industrial chimneys and vehicle exhaust systems to create turbulence and improve the mixing of airborne pollutants, which can help lower emissions and increase combustion efficiency.

8. Bluff bodies are used in chemical reactors and mixing chambers to create turbulence in order to improve the mixing of different fluids or chemical species.

9. Wind power: To effectively capture wind energy, bluff bodies are used in the blade design of wind turbines. The aerodynamic characteristics of bluff bodies affect the performance of wind turbines.

10. The hydrodynamics and stability of boats, ships, and submarines are significantly impacted by bluff bodies in the design phase.

e) Hydraulic diameter

Hydraulic diameter, a term from fluid mechanics, describes the "size" or "effectiveness" of a non-circular duct or channel through which a fluid flows. It is particularly useful for managing flow through ducts or pipes with non-circular cross-sections, such as those that are rectangular, triangular, or irregular in shape.

The hydraulic diameter (h_d) is calculated as four times the ratio of the cross-sectional area (A) of the duct to the wetted perimeter (P) of the duct. Mathematically, it is expressed as:

h_d= (4*A)/P

Where:

h_d is the hydraulic diameter,

A is the cross-sectional area of the channel, and

P is the wetted perimeter.

f) Calculation of hydraullic diameter

There is an octagonal bluff body of each side, which is D =0.42 cm

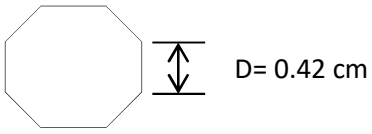

$$h_d = \frac{4A}{P} = \frac{4[2(1+\sqrt{2})D^2}{8[D]} = \frac{4[2(1+\sqrt{2})0.42^2}{8[0.42]} = 1.0143 \approx 1 \text{ cm}$$

g) Orientation of the thesis

The orientation of a thesis titled "Numerical Simulation of flow and Heat Transfer around an Octagonal Bluff Body" would likely be within the field of mechanical engineering, specifically focused on heat transfer, and computational fluid dynamics (CFD).

There are six chapters in the present thesis.

In Chapter 1, the distinction between a bluff body and a stream line body, their applications, the flow field, and their classifications have all been briefly discussed.

In Chapter 2, include a thorough literature evaluation of the complete thesis, explaining how it assisted the research in terms of methodology, technicality, and math.This comprises of a review of the literature on numerical simulations surrounding bluff bodies, vortex flow surrounding bluff bodies, and channel wall augmentation. The objectives of the literature survey were listed in the last section of chapter two.

In Chapter 3, focuses on the computational technique modeling in mathematics that is used in the current study work. The explanation of parameters used to measure performance includes the surface averaged Nusselt number and the shape of the simulated flow.

In Chapter 4, analyzes transportation phenomena around bluff body shapes. This investigation also examines the impact of turbulence intensity on heat transfer across a wide range of Reynolds numbers, including unstable governments. Additionally, the impact of TI on drag and pressure coefficients is investigated here.

In Chapter 5, various parameters are used in the analysis of results and discussions.

In Chapter 5, explains briefly the conclusion reached based on the study's analysis. In this chapter, future study prospects are also mentioned.

Chapter 2

2. Literature review

The main objective of this paper is to analyze flow past a circular cylinder in two and three dimensions under various laminar flow regimes. This simulation uses an implicit pressure-based finite volume method for time-accurate computation. Convective flux discretization methods for incompressible flow with second order precision. Aerodynamic coefficients' range for the periodic unsteady flow regime. **Rajani et al. (2009)** focused for both two- and three-dimensional flow, the wake structure behind a circular cylinder has been calculated using the second order accurate implicit finite volume Naiver-Stokes solver RANS3D. Reynolds numbers between 0 and 400 have been calculated to fall into three different characteristic regimes. The main physical properties of the flow in different regimes are fairly accurately captured by the current computation method. This demonstrates the RANS3D flow solution algorithm's sufficiency and accuracy. Up to Re 14 200, the results of the two-dimensional calculation are in a fair amount of agreement with the precise measurement data for the Strouhal number. At the critical Reynolds number of 180, which denotes instability, large discrepancies have been observed between the results of the two-dimensional flow computation and the measurement data for the Strouhal frequency and amplitude. In the current computation of the three-dimensional flow, all have been considered. The calculated stream wise and span wise vortices component contours show a less regular and less aligned wake structure for Re > 250 on various Cartesian planes and the shorter wavelength of the stream wise vortices. The computations make use of a larger domain and a finer resolution and a way to better comprehend the physics of the transition process in the wake of the cylinder. **Mallick and Kumar (2014)** have described that Drag is the main consideration in aerodynamic design. The drag coefficient was for a cylinder. Based on data gathered from experiments performed in an air flow bench (AF12) with varying flow rates and diameters of 12 mm, 15 mm, 20 mm, and 25 mm. There must be two values found for the drag coefficient. Both direct weighing and cylinder-pressure distribution have been employed as techniques. Two analysis techniques were used to determine the drag measurements on the cylinder. Comparisons have been made between the drag coefficients obtained using the two methods. The drag coefficient is found to be noticeably off in two values. The drag coefficient obtained by the weighing method is more precise when compared to those obtained through pressure distribution. The drag force increases along with the increase in cylinder diameter. Additionally, it has been found that for cylinders of a certain diameter, the drag force increases as air velocity increases. Once more, direct weighing and was used to determine the values of the drag coefficient. In the range of angle of incidence between 0 and 180o, pressure distribution profiles exhibit good agreement. Compared to the other two approaches, pressure plotting yields are the most reliable. In this experimental study, we characterize the instantaneous vortices and time averaged velocity, vortices, root mean square (rms) velocities, Reynolds stress correlations, and phase-averaged contours in the downstream of circular, sharp-edged square, and 45° oriented square cylinders in a uniform flow. Strouhal numbers for 550 Re 3400 are computed using wake

flow patterns. Shear layers encircling the recirculation bubble region behind the cylinder are discussed with regard to flow physics and the lengths of large-scale K'arm'an vortices. The extents to which cross-stream velocity correlations with Reynolds stress are improved are made clear by **Muammer Ozgoren (2006).** For each of the patterns displayed, the lengths of the vortex formations tend to decrease as the Reynolds number increases. The current results can reveal enough information about the aforementioned flow features to help formulate a plan for the future validation of numerical models. **Saeedi et al.(2014)** have studied the turbulent wake behind a square cylinder mounted on a wall with an aspect ratio of 4, and a Reynolds number of 12 000 (based on the free-stream velocity and obstacle side length), is investigated using direct numerical simulation because the has a high aspect ratio and a relatively high Reynolds number. When tested on a cylinder, the wake is dispersed widely behind the cylinder and exhibits complex, vigorous vortex motions. The patterns of lateral and tip vortex shedding at different frequencies, coherent structures downstream of the obstruction, rate and distribution of turbulent kinetic energy, and instantaneous pressure distribution in the wake region are all investigated in great detail. In order to validate the numerical results, the first- and second-order flow statistics derived from the simulations have carefully been compared against the available wind-tunnel measurement data. **Richter and Nikrityuk (2012)** perfomed the study, this study focuses on numerically simulating the flow of fluid and heat past a variety of spherical and non-spherical particles. Studies of Nusselt number (Nu) relations for non-spherical particles are rare compared to studies of drag forces (cd) for spherical and non-spherical particles. It is motivated by this fact to consider cuboid, spherical, and ellipsoidal particles in steady-state regimes with Reynolds numbers (Re) ranging from 10 to 250. Due to the asymmetric flow that develops as Re approaches the value of 250, all simulations are run in three dimensions. A good agreement was found between our numerical results for the sphere and published values for drag coefficients and Nusselt numbers. The analysis of the numerical outcomes for non-spherical particles showed that, in addition to the Reynolds number, three other geometry parameters also influence the interaction between particles and fluids: the drag coefficient is primarily dependent on normalized longitudinal length, while sphericity and crosswise sphericity influence the Nusselt number. As a result, new correlations between the Nusselt number and the drag coefficient are established. The precision of the closures developed for cd and Nu is discussed in comparison with published models. The aerodynamic characteristics of a square prism in a uniform flow for various angles of attack have been used the LES turbulence model to investigate. The findings show that for all angles of attack, mean aerodynamic coefficients, surface pressures, and flow patterns are in good agreement with the outcomes of experiments. The spanwise size of the computational domain has also been found to have a negligible impact on the mean aerodynamic. The fact that it exhibits strong impacts on fluctuating aerodynamic coefficients but has little effect on constant aerodynamic coefficients serves as the inspiration for the development of a grid-independent estimation method for quantitative evaluations of fluctuations. Successfully capturing the abrupt change observed around 141, the strouhal numbers derived from the simulations are in good agreement with the experimental results. Last

but not least, a technique for estimating fluctuating aerodynamic coefficients independent of the grid is proposed and validated by means of a systematic elongation of span wise length tests that are numerical. **Shinichi Oka and Takeshi Ishihara (2009)** have performed the span wise length of the computational domain has a significant impact on varying aerodynamic coefficients but little impact on mean aerodynamic coefficients. It is found that the span wise length of 1D is practically adequate. A method for estimating grid-independent fluctuating aerodynamic coefficients is proposed in order to increase the precision of the predicted fluctuation obtained by using smaller span wise length, which in turn reduces cost and memory for the simulations. It should be noted that the proposed method only requires a numerical model with a span wise length of 4D, whereas the ideal span wise length for the conventional approach is 20D. It has been possible to study the nature of flow development in a parallel plate channel by using an intermittent model that was just developed. Together, the model and those equations constitute momentum conservation, the continuity equation, and the SST turbulence model were used to provide a complete chronology of the development processes and the derived practical outcomes. How inlet conditions influence the developing flow's behavior downstream is the main area of interest in this work. It was found that the turbulence intensity and the shape of the velocity profile represent the specifics of the inlet conditions, which have a significant impact on how the flow develops. The velocity profile shapes with flat and parabolic shapes are thought to be limiting cases. Similar to this, the turbulence intensities Tu = 1% and Tu = 5% are employed. From a practical standpoint, there is a significant correlation between the friction factor and Reynolds number. In the other cases (flat profile, Tu = 1%, and parabolic profile, Tu = 1% and 5%), the breakdown of laminar flow takes longer, and at Re 10,000 full turbulence begins rather abruptly. There are three distinct, fully developed flow regimes that may exist depending on the circumstances at the inlet and the Reynolds number. In addition to the usual laminar and fully turbulent regimes, another one called fully developed intermittent can also exist. In the latter regime, laminar and turbulent flows specifically alternate. **Minkowycz et al. (2009)** have observed both the inlet circumstances and the Reynolds number's value have an impact on how the flow patterns evolve along the channel's length. Specifically, three different fully developed regimes have been identified. The inevitable outcome of flow development for higher inlet turbulence intensity levels is a new flow regime known as fully developed intermittent in addition to the well-known laminar and turbulent regimes. In fact, even for the lowest of the considered turbulence intensities (1 percent), the fully developed intermittent regime was observed for specific Reynolds numbers in the case of a flat inlet velocity profile and Tu = 5%), the fully developed regime's type went from laminar to intermittent to completely turbulent continuously as a function of the Reynolds number. The outcomes of turbulent heat and fluid flows in a straight square duct (SSD) at higher Reynolds numbers, ranging from 104 to 106, are presented in this paper using large eddy simulation (LES). The bulk mean velocity and the side length of the duct's cross-section are the foundations for these findings. The suggested sub-grid model makes the assumption that the sub-grid stress and heat flux are proportional to the temporal increments of the filtered strain rate and temperature gradient, respectively, with the

proportional coefficient being determined by calibrating the friction factor. The temperature was believed to be passive because the buoyancy effect was disregarded. The results show that LES results are superior to c-DNS results, and Kolmogorov scales in the SSD are predicted. The LES results reveal that the largest relative deviation of the overall mean Nusselt number is less than 10% in comparison to the experimental correlations that are currently in use, which helps to explain why the c-DNS is applicable to the issue at a moderate Re. Empirical mode decomposition (EMD) was used to examine the fluctuation of the cross-sectional origin with temperature at Re 14 105, which is the x-averaged value studied by **Zhu et al.(2010)** Pressure and velocity fields around rigid prisms with rectangular cross sections are numerically simulated for a Reynolds number of 105 using the large eddy simulation (LES). LES and a finite difference scheme based on a staggered grid are used, and the convection terms are discretized by the QUICK scheme. A computationally efficient tool for simulating high Reynolds number flows around bluff bodies is provided by this numerical scheme and the LES model. The LES scheme used in this study can be viewed as a coherent structure capturing method, which can be distinguished from a true LES where the scales are typically resolved to very small size. The mean and root mean square (RMS) values, as well as the power spectra of the pressure variations on the prism surface, are also included. Present are the probability densities for integral forces (lift and drag forces) and pressure fluctuations. The chord wise correlation of pressure and the eigen function expansion of the square prism are discussed in more detail. Then, by additional researchers, simulation results are compared with the available experimental data and numerical results, including the mean velocity along the symmetry line. With the exception of the probability densities, for which there were no experimental data available, and the lift and drag force spectra, whose values do not closely match, all other features are observed to be in good agreement with experimental results. The integral lift force on the bluff body sheds two vortices every cycle, according to crystal-clear streakline sequences. There are separation-reattachment patterns on the side faces of rectangular prisms also seen. A parametric analysis of bodies with different aspect ratios serves as an illustration. Streamwise length has a significant impact on the flow field patterns, which is evident. **D. Yu and A. Kareem (1996)** have illustrated the flow field's vortical structure and the characteristics of rectangular prisms with different aspect ratios are both well-illustrated by the study's streaklines. The qualitative patterns of pressure distribution alongside faces of the streaklines are consistent with the simulated pressure distribution around prisms. This grid refinement analysis reveals that while the pressure on the square's upstream face remains constant, there are some differences in the separated regions. However, the characteristics of the simulated pressure field closely resemble the experiment's results. **Ju Yeol You and Oh Joon Kwon (2012)** have presented the main objective of this study is to evaluate the performance of different turbulent models in simulating flow around a cylinder at a critical Reynolds number (Re = 8.5105). Two equals 0 point 7 percent. Three different flow features were simulated using a hybrid RANS/LES model (SAS model), a correlation-based transition model, and a fully turbulent RANS model (SST model), including the laminar-turbulence transition inside the boundary layer and the unsteady vortex shedding in the wake

region. They successfully demonstrated their applicability for the flow simulation at a crucial Reynolds number regime. The computational domain was discretized using an unstructured mesh method, and the incompressible Navier-Stokes equations were discretized using a vertex-centered finite-volume method. Inviscid fluxes have been evaluated using 2nd-order Roe's flux difference splitting, and viscous fluxes have been computed using the central method. Dual time-stepping and the Gauss-Seidel iteration were used to perform unsteady time integration. A parallelization technique utilizing the METIS and MPI libraries was used to reduce the cost of computation. We compared turbulent models' unsteady characteristics and time-averaged quantities of the flow fields. The results of the experiment were compared to the numerical results. The turbulent models produced remarkably different results at the critical regime because each model has a different ability to predict different flow features, such as laminar-turbulence transition and unsteady vortex shedding. **Stringer et al. (2014)** performed the test to use a methodology for calculating flow around spherical cylinders. Both the CFX-13.0 by ANSYS and the 1.7 by OpenFOAM are well-known commercial and open-source solvers. Solutions for flows with Reynolds numbers that take a variety of diameters and flow conditions into account. To maintain realistic solve times, a 2D Unsteady Reynolds-Averaged is necessary. This method is known as Navier-Stokes (URANS). In order to maximize accuracy, a carefully watched meshing technique, suitable adaptive timestepping, and a suitable turbulence model are put together. Despite the nearly identical case definitions, there are noticeable differences in the results between solvers. OpenFOAM performs better at high sub-critical and critical values while ANSYS performs better at low to sub-critical values. Because the developed methodology eliminates many common variances related to the grid and transient components of URANS computations, it can be used as a benchmark case for additional codes solving cylindrical structures. Numerous engineering and industrial applications make use of a significant phenomenon that occurs over a circular cylinder. It is a challenging case because the complex flow regime includes close-to-the-cylinder laminar separation, turbulence, reattachment, and vortical motions. The ability of the RAST model, a zero-equation sub-grid scale (SGS) model, to forecast the flow characteristics surrounding a spherical cylinder at ReD = 3900 is assessed in the current study. This SGS model can be used to simulate flows with strong separation and recirculating in a subtle way because it is sensitive to non-equilibrium flows and maintains the anisotropic features of turbulence. The comparisons show that, especially close to the cylinder's wake, the RAST model is capable of accurately simulating mean flow characteristics that are in strong agreement with the outcomes of previous experiments. RAST in comparison to DSM. The model only needs one filtering step, which more fully recovers the computational effort and numerical stability. **Taghinia et al. (2015)** have concluded both models to better account for non-equilibrium effects encountered. The RAST model consistently outperforms the DSM in terms of prediction accuracy, which improves agreement with experimental data. In the vicinity of a cylinder, this is demonstrated. Furthermore, because it retains the single grid-filter feature, the RAST model is superior to the DSM with grid-filter and test-filter scales. The RAST model in the incompressible code requires roughly as much computational work as all of the

simulations combined roughly 70-80% of the cost of the DSM. Comparably priced to the Smagorinsky model is the current design. An LES can naturally use the RAST model, which forecasts the unsteady forces, mean component, and fluctuating component, to compute bluff-body flows. The supercritical to upper-transition flow regimes around a two-dimensional (2D) smooth circular cylinder have been numerically investigated using 2D Unsteady Reynolds-Averaged Navier-Stokes (URANS) equations with a typical high Reynolds number k 3 turbulence model. The current study aims to investigate the model's applicability for internal engineering design. Anisotropic turbulence is successfully designed in high Reynolds number flows around a smooth circular cylinder in the supercritical and upper transition. The flow around a 2D smooth circular cylinder has been computed using high Reynolds numbers covering the supercritical to upper-transition flow regime in addition to the 2D URANS. The current study demonstrates that for engineering design purposes, this model gives satisfactory qualitative agreements with the published experimental data and numerical results in the supercritical and upper-transition flow regimes, despite previous research showing that it provides less accurate predictions of flow with strong anisotropic turbulence. Additional experimental data, particularly measurements of the Reynolds stress profile and velocity outside of the supercritical flow regime, are required to conduct a more thorough validation study of the model. In the interim, the current study should be dependable and useful as a tool for evaluating engineering design work illustrated by **Ong et al. (2009).** The investigated pressure fields surrounding a rectangular prism using a novel turbulence-generation method. The uses jets that are blowing laterally away from the main flow and against stationary obstructions. The findings that are presented here are the preliminary findings. Phase of a research project to investigate the effects of turbulence on the aeroelastic stability of long-span bridges. As a result, measurements were taken in a range of flows while varying the integral scale and maintaining a constant level of turbulence observed by **Fred et al. (1998)** and concluded the shed light on the relative effects of small and large scales, tests of a different type than those described here will need to be conducted. The turbulence-generation technique presented here provides a novel way to modify the relevant statistics. The research that comes after will examine pressure correlations along the stream and the span, simultaneous measurements of pressure and velocity, and dynamic testing to examine how the turbulence scale affects flutter derivatives. **AFRREV STECH (2013)** has shown the effect of irregular flow around a rectangular cylinder has been the subject of extensive scientific study for many years. A two-dimensional unsteady flow is created by pasting. The rectangular cylinder has been mathematically examined for the low Reynolds numbers (flow is laminar). Fluent was used to create the geometry and meshes for this project, also Fluent was used to conduct the computational fluid dynamics analysis. The effects of the pressure distribution and vortical structure on the region surrounding rectangular cylinders are investigated and reported. The integral aerodynamic parameters are also included. It is advised that more research be conducted in order to confirm the current hypothesis and fully comprehend the fundamental fluid flow phenomena that drive the aerodynamics section and provide a comprehensive database for verification and comparison requirements. If both are adopted by the scientific community, the

benchmark might offer a helpful framework for future research approaches that combine experimentation and computation. **Toukir Islam and S.M. Rakibul Hassan (2013)** observed the flow past a stationary circular cylinder at Re=10^5 is numerically investigated using the Favre-averaged Navier-Stokes equation and the finite volume method. Numerical observations are used to compare experimental findings to other researchers' research pressure distribution and flow separations are just two examples of the many flow phenomena. Drag surface, vortex shedding, etc. Additionally studied are various boundary conditions. Along with a brief comparison of the 2D and 3D numerical calculations, extensive research is done on the nature of the vortices distribution and the effects of surface roughness. Between 80 to 90° degrees from the stagnation point upstream on either side of the cylinder. The drag coefficients for smooth surfaces are 0.533 and 0.771, respectively. Numerical calculations in 2D and 3D, respectively, and the resulting changes in drag, are used to illustrate the effects of surface roughness on drag. Estimates for surface roughness and drag coefficient are 0.004 and 0.43, respectively. Even though the wake structure is barely visible, they are not as common as in Karman Street. For a clearly defined relative roughness, boundary layer transition happened at Re as low as10^5. Asymmetry in the distribution of vorticity parallel and perpendicular to the flow directions has been found, and this could cause vibration as well as a lift or drag force. Future researchers ought to concentrate on a select few specific areas. In order to investigate the impact of surface roughness on flow parameters experimentally, a cylinder with a specific surface roughness was used in the experimental section, and various surface roughness would be recommended. The correlation between surface roughness and the separation angle may also be of interest to future researchers. **Ravi Golani and A. K. Dhiman (2014)** presented the movement of fluid past an obstruction with a circular cross-section is a classic example of a fluid mechanics problem. In this investigation, both fluid flow and heat transfer were examined. A two-dimensional circular cylinder is taken into consideration in the unsteady flow regime. Drag and lift coefficients are affected by the Strouhal number, Reynolds number, and heat transfer properties of the vehicle. Investigations are conducted for a long, heated, circular cylinder with Re = 50–180 (in steps of 10). The Prandtl number is equal to 0.7 (air) in the unconfined unsteady cross-flow. Numerical simulations have been used to accomplish it. To display flow patterns, the instantaneous streamline, vortices magnitude, velocity magnitude, and are used. Experimental and numerical data for a circular cylinder can be found in the literature as a result of heat transfer. The average Nusselt number increases as the Reynolds number increases similar to the Reynolds number. The rms drag and lift coefficients, however, do not rise in proportion to the drag coefficient and shedding frequency as the Reynolds number rises. And finally, a simple relationship between the drag coefficient and the time average. The Nusselt number is calculated as a function of Reynolds number for the variety of conditions covered by this study. The instantaneous streamline, vortices size, velocity size, and are used to display the flow pattern. Distributions of pressure inside the spherical cylinder with an increase in Reynolds number, the drag coefficient decreases. However, while the shedding frequency doesn't change with Reynolds, the rms drag and rms lift coefficients. The precise temperature fields near the obstruction can be seen in

isothermal instantaneous profiles. It displays the temporal evolution of the average Nusselt number. As a function of Reynolds, there is a correlation between the time-averaged drag coefficient and the time-average Nusselt number. For the variety of conditions included in this study, a number is obtained. **Islam et al. (2014)** provided detailed time-trace analyses of the drag and lift coefficients, power spectra analyses of the lift coefficient, and vortices contours phase diagrams, visualizations, and streamlines calculated and contrasted with numerical outcomes and sharp experimental data discovered in open literature. Reynolds numbers had an influence on physical quantities. In order to validate the code and analyze some significant flow features around a square cylinder for Reynolds numbers ranging from 80 to 200, this paper suggests a two-dimensional numerical study using the multi-relaxation-time lattice. The present study also predicted the effects of Reynolds numbers on physical quantities such as drag coefficient, mean drag coefficient, Strouhal number, and root-mean-square values of drag and lift coefficients. When compared to other experimental and numerical outcomes, the predicted numerical results for the chosen computational domain show a positive trend. They saw a satisfactory agreement between the experimental results and the current numerical data at low Reynolds numbers. It was also found that the physical parameters could be altered by altering the Reynolds numbers. A two-dimensional rectangular prism with a fineness ratio (chord-to-thickness) of 5.0 is used to study the unsteady flow field surrounding it using unsteady Reynolds-Averaged Navier-Stokes (URANS) equations. The presentation of a grid-convergence study explores how the flow solution depends on the spatial and temporal discretization. The strong Reynolds number effects observed in wind tunnel tests will also be investigated using numerical simulations. However, only the turbulence model based on the EARSM approach was able to capture the significant lift increase at non-zero angles of attack due to variation in Reynolds number. For several test cases, satisfactory agreement with wind tunnel data is obtained. On one side of the rectangular cylinder, it is shown how the time-averaged shear-layer reattachment location has slowly migrated upstream. Finally, this work demonstrates that predictions for massively separated flows, which present a significant challenge for CFD, can be made with reasonable accuracy. Additionally, the numerical simulations can qualitatively and quantitatively replicate the physical behavior and provide an explanation for it. However, it is clear that the two-dimensional URANS method can only accurately simulate unsteady bluff-body flows to a certain degree. The analysis of the shows that more complex three-dimensional techniques, like Large-Eddy Simulation and Detached-Eddy Simulation, can be used to make even more advancements. In the future, using these state-of-the-art methods, it will be fascinating to investigate the important Reynolds number effects that are observed for this cylinder geometry when a small angle of attack is imposed and studied by **Mannini et al. (2010).** The numerical analysis of flow past a square cylinder at a Reynolds number of 21,400 was done using the large-eddy simulation technique. Using a dynamic sub grid-scale stress model, the small scales of turbulence were simulated. It is also possible to forecast how turbulent normal and shear stresses will be distributed. The relative sizes of the coherent and incoherent components of turbulent fluctuations at some defined phases have been compared upstream of the cylinder. While the magnitudes of the coherent and

incoherent components are similar in the far wake, coherence is greater in the near wake than the far wake. **Srinivas et al. (2006)** predicted time-averaged flow performs well when compared to both the experimental results and the results of the published LES. The turbulent normal stresses and shear stresses are fairly well predicted by the current LES computations. Although the near wake has higher levels of coherence than the far wake, both coherent and incoherent components are of comparable size there. When the shed vortices of the near wake are broken up, the cascade mechanism of energy transfer is formed as the turbulent flow grows. **Catalano et al. (2003)** has studied the viability and accuracy of large-eddy simulation (LES) with wall modeling for high Reynolds number complex turbulent flows, the flow around a circular cylinder in the supercritical regime is taken into account. A straight forward wall stress model is used to broadly define the boundary conditions for the LES. It is shown that the LES answers are considerably more accurate than the RANS results. They accurately depict the delayed boundary layer separation and lower drag coefficients that follow the drag crisis, which are in line with experimental measurements. The mean pressure distribution is predicted reasonably well for $Re_D = 5 \times 10^5$ and 10^6. Because the Reynolds number dependence is ignored, the solution loses precision with higher Reynolds number. In comparison to the need to resolve the outer boundary layer scales, it should be noted that the grid used near the surface, especially before separation, is quite coarse. In the laminar region and with coarse grid resolution, the boundary layer's behavior is not entirely clear. A more thorough investigation is needed to differentiate between the effects of the grid resolution and the wall modeling as well as to fully validate the numerical approach for this challenging flow. **Ruith et al. (2004)** studied the appropriateness of various open boundary conditions is evaluated for direct numerical simulations. Domains of infinitely long, incompressible, spatially evolving, and time-varying swirling laminar jets in the downstream and radial directions. Due to the fact that this class of flows can support traveling waves, it is particularly challenging to specify conditions for them at open boundaries. This is done by setting up and testing a number of radial boundary conditions, such as a free-slip condition, two different homogeneous Neumann conditions, and a radiation condition inspired by the outflow boundary condition, to see how well they can maintain local and global mass, handle low and high entrainment flow, and handle artificial waves that don't propagate from the boundaries into the interior. The global mass is automatically conserved in the free-slip and simple to the accuracy of the machine. The free-slip condition typically requires the largest radial extent of the computational domain due to its impermeable nature and difficulties with high entrainment flows. As a result, it has been discovered that the radiation condition serves as the lateral boundary condition that is most favorable for both high and low entrainment jets. The lateral boundary for the low entrainment case looks like a stream surface even at relatively small radial distances. The outcomes of the free-slip and radiation conditions under these conditions are almost identical as long as the radial boundary is positioned at a sufficiently large distance. The radiation condition approximates the true physical solution even when the radial boundary is two characteristic core radii from the axis, whereas in this extreme case, the free-slip condition significantly underestimates the bubble size. Thus, the radiation condition is the most

advantageous choice for both high and low entrainment jets. **Ravi et al. (2012)** have shown at smaller angles of attack, rapid changes take place. It renders the speed and direction of the incoming flow. The structure of the instantaneous flow has significantly changed over the airfoil, leading to a significant increase in surface pressure fluctuations. The leading edge's roll up was enhanced and the shear layer was separated, which produced a noticeably different flow field over the airfoil at higher angles of attack. Leading Edge Vortices had a significant influence and a deciding element in the aerodynamic loads experienced. Time-varying surface pressure measurements were taken at a variety of chord wise stations to study the flow structure over a thin airfoil. Although the turbulence intensities in the two turbulence conditions were noticeably different, the longitudinal integral length scales were nominally the same. For the design of these structures, scaled-model wind tunnel tests are frequently required. In order to study the aerodynamic behavior of a bluff body, the tower section of a cable-stayed bridge is used in the paper. In particular, the effects related to the turbulence intensity of the incoming flow are the focus of the wind tunnel tests, which employ a rigid sectional model. When examining bluff bodies, it is well known that the drag coefficient depends on the Reynolds number during the experimental campaign, a cable stayed was used. Although a wide range of wind speeds has been investigated for the bridge tower, no appreciable Reynolds has been discovered. Numerous effects have been discovered. But there is a sizable reliance on the small scale. The location of the turbulent incoming flow has been made clear, especially for some exposure that has undergone testing. It has been observed that even a small increase in turbulence intensity can completely change angles and reduce the phenomenon of vortex shedding. Additionally, the author claims that the aerodynamic behavior of the model is influenced by the length scale of the turbulence in relation to the distinctive dimension of the section under consideration studied by **Belloli et al. (2012). Sun et al. (2016)** have shown the effect of the optical characteristics of diatom chains in the ocean, the many-body iterative T-matrix (MBIT) method and the ray-by-ray (RBR) geometric optics method are combined. The numerically precise MBIT method is useful for scatters with linear cells. In contrast to other widely used geometric optics techniques, the approximate RBR method accounts for the interference of all rays that are sent out. The two approaches are verified in comparison to benchmark simulations. Any optically soft particle, i.e., can be simulated using either method—or both—to simulate diatom chains of different sizes as the relative refractive index approaches unity. Two-dimensional simulations of ocean chains are used. The RBR is an approximation method, while the IITM and MBIT are numerically accurate techniques. The applicability of the three methods to diatom chains is confirmed by comparing simulations based on the ADDA and PGOH methods. The refractive indices and particle model were developed based on the actual shape and composition of diatoms. The interference is necessary to get logical outcomes. The rays that are emitted between soft particles must be considered. The MBIT efficiently handles linear diatom cell chains thanks to the one-cell transition matrix and iterative technique. There are many diatom cells that use the RBR. The results are then applied to all other cells in terms of the periodic boundary conditions after one cell has been traced. **Prhashanna et al. (2011)** have made a study thorough numerical simulation

for the 2-D laminar flow of fluids over an equilateral with power laws. Triangular cylinder experiments are carried out to more fully comprehend the impact of the power-law index on the critical Reynolds number indicating the start of flow separation and vortex shedding and apex of the triangular cylinder facing both upstream and downstream directions in contrast to Newtonian. A triangular cylinder's phenomena and heat transfer characteristics for shear-thinning fluids have been studied in the steady flow regime. The pressure and total drag coefficients in the steady flow regime decrease as the Reynolds number rises in spite of everything. The power-law index's influence gradually lessens with increasing Reynolds numbers. Shear-thinning is seen to facilitate heat transfer under similar but otherwise unchanging circumstances. As a result, heat transfer can be increased by 50 to 60 percent in comparison to Newtonian fluids at the same Reynolds and Prandtl numbers. **Wang et al. (2012)** derived the hydraulic diameter of the obstructed section, which is determined as the ratio of the total wetted surface area to the flow-available open duct volume, was varied from Reynolds number 4800 to 8200. In comparison with circular pin fins, the more streamlined drop-shaped pin fins were better in delayed or suppressing separation of the flow passing through them, which reduced the aerodynamic cost. The circular pin fins improved heat transfer more than the drop-shaped pin fins, but not as much. Drop-shaped pin fins are a viable alternative design to circular pin fins in terms of key performance metrics. Experimentally and numerically, the flow and heat transfer characteristics within a rectangular channel lined with pin fins were examined. In a staggered arrangement, many pin fins with various shapes—including circular, elliptical, and drop-shaped—but identical cross-sectional areas have been evaluated. The research on the flow and heat transfer process of a rectangular channel placed with staggered pin fins is analyzed in this paper using computational and experimental results. The heat transfer of drop-shaped pin fins is weaker than that of circular pin fins. The reduction in average Nusselt number between the drop-shaped and circular pins was about 24% for drop-A, 26% for drop-B, and 27% for drop-C. **Ro (2015)** has measured lift and drag and visualizing the flow field using particle image velocimetry, the properties of the flow field surrounding a square prism with a small triangular prism upstream were examined. Triangular prism to square prism width ratio (H/B, where H and B are the side lengths of the respective triangular and square prisms) and triangle prism to square prism gap ratio (G/B, where G is the gap distance between the respective triangular and square prisms) were experimental characteristics. The side length of the triangular prism and the separation between the fronts of the square and triangular prisms were set as variables in this study, which substituted a triangular prism for a circular prism or a vertical plate. Fluid force measurements were used to examine the square prism's features for reducing drag and lift. Particle visualization was used to examine the gap ratio resulting in a pretty high drag reduction rate. The lift reduction rate of the square prism, with an average lift reduction rate of 52.4%, was barely influenced by the width and gap ratios of the triangular prism. As the gap ratio went further, the Strouhal number for the square prism first increased, and then diminished. In the presence of the triangular prism, stagnation regions developed in the upstream and downstream regions of the square prism; their size rose in the upstream region and reduced in the downstream region with increasing width ratio. By

measuring the lift and drag on the square prism and visualizing the flow field using PIV, the characteristics of the lift/drag reduction and flow field that act on the square prism were studied with a fixed Reynolds number Re=1.0 104, H/B = 0.2, 0.4, and 0.6, and G/B = 0.0-3.0 in increments of 0.5. **Dhiman and Aggrawal (2016)** have shown the flow exhibits a time-periodic characteristic throughout the whole range of control parameters investigated. For pseudo-plastic and Newtonian fluids, an increase in Re is seen along with a corresponding increase in the time-averaged total drag coefficient. When the time-averaged total drag coefficient is modified with n for dilatant fluids, a mixed trend is shown. For dilatant fluids, the value of the Strouhal number increases as Re rises, however a mixed trend of the Strouhal number and Re is seen for pseudo-plastic fluids. The handling and processing of non-Newtonian fluids, such as diluted polymer solutions with smaller molecules, starch solutions, syrups, foams, slurries, polymer melts and solutions, paper and pulp materials, and others, that exhibit pseudo-plastic (shear-thinning) and/or dilatant (shear-thickening) behavior, requires the knowledge and skills of chemical and process engineers. The literature has grown to include an enormous quantity of computational and/or experimental data on the flow properties of power-law fluids past an obstruction with a circular cross-section. Moreover, the other obstruction, a square prism, has been fully studied in the literature, and sufficient details on the flow of power-law fluids around a square-cross-section prism in both a steady-state and unsteady flow regimes can be found elsewhere. On the other hand, it is difficult to find many books that address how these fluids flow over a triangular cylinder-shaped prism, as is the case in the next paragraph. Therefore, the current work conducts a study of the unsteady laminar flow across a triangular prism in an unconfined domain. They investigated the varying ranges of power-law indices (n) and Reynolds numbers (Re) in the unbounded and time-periodic flow of non-Newtonian power-law fluids around an equilateral triangular prism. Significant numerical outcomes are attained, including total drag and lift coefficients, a mixed trend of time-averaged drag coefficient rms values of drag and lift coefficients, and Strouhal number. Streamline contours around a triangular prism are used to illustrate the specific fluid flow characteristics. For every control parameter examined in this article, there is a time-periodic flow. With an increase in Re, the time averaged drag coefficient rises for Newtonian and pseudo plastic fluids.

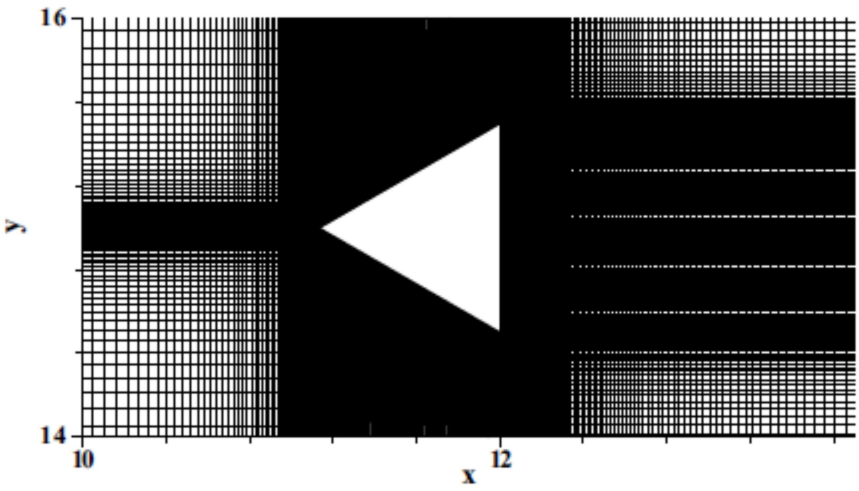

Fig. 2: Grid structure around an equilateral triangular prism (magnification view)

In this study, the effects of wall confinements (or blockage ratios) on the flow and heat transfer characteristics around a long, equilateral triangular bluff body placed in a horizontal channel for Reynolds numbers (Re) ranging from 1 to 80 and blockage ratios ranging from 0.1 to 0.5 for air as the working fluid are the main topics of study. The commercial solver Ansys Fluent, which is based on the finite volume approach, is used to solve the governing continuity, Navier-Stokes, and energy equations as well as the relevant boundary conditions. Because the channel walls apply an extra retardation force to the obstacle, the total drag coefficient falls with an increasing value of Re for a fixed value of the blockage ratio, but it increases with an increasing value of the blockage ratio for a fixed value of Re. As the blockage ratio's value rises, flow separation takes a while to begin. The flow around sharp-edged bluff bodies has been intricate and interesting over the past ten or more decades. As a result, a huge number of study papers have been generated and drawn to this flow scenario. Its engineering importance in relation to structural design, energy conservation, acoustic emissions, flow metering devices, cooling of electronic components, and other applications is the fundamental reason for this are carried by **Dhiman (2016)**. Calculating the field variables and related values, which are then utilized to calculate the drag and lift coefficients as well as the Strouhal and Nusselt numbers, has been the main focus of these investigations. For Re = 1 to 80 and β of 0.1, 0.125, 0.25, and 0.5 at the Pr of 0.71, the effects of wall confinements on the flow and heat transfer properties of a long confined equilateral triangular cylinder have been examined. The flow and temperature fields close to the triangular obstruction are defined for various using the streamline and isotherm contours. Because the channel walls apply an additional retardation force to the triangular cylinder, the total drag coefficient drops with an increase in the Re for a fixed value of , while it increases with an increase in for an expected value of the Re. For a fixed value of , the average Nusselt number rises as Re rises. Finally, for the previously discussed range of values, simple correlations for wake length, total drag coefficient, and average obstacle Nusselt number are determined. **Chatterjee and Mondal (2012)** have performed the computational domain has been

separated using an unstructured triangular mesh, and Fluent, a commercial CFD solver, is utilized to run the simulation. At different Reynolds numbers, the streamline and isotherm patterns are used to study the flow and heat transfer characteristics. The drag coefficient, Nusselt numbers, and the dimensionless frequency of vortex shedding (Strouhal number) are all presented and analyzed. The results obtained are in strong agreement with the results that are already available in the literature. The streamline, vorticity, and isotherm contours provide as an image of the hydrodynamic and thermal fields' typical behavior. The drag and lift coefficients, Strouhal number, and Nusselt number, as well as other global flow and heat transfer variables, are computed and explained. Finally, given the specified set of conditions, a straightforward heat transfer correlation is derived, showing the functional dependency of the Colburn j-factor with the Reynolds number. These numbers may be helpful in determining the average Nusselt number from an a priori Prandtl number prescription. The distribution of the isotherms on the back surface has a greater effect as the Reynolds number rises. Although the isotherm profiles differ significantly with Prandtl numbers and the amplitude of oscillations of both the drag and lift coefficients increase with Re, the overall flow pattern varies independently of Prandtl numbers. The Strouhal number rises more quickly up to Re = 100, then more slowly until it reaches its peak at approximately Re = 150.

In this research, **Nakayama et al. (1996)** have performed vortex shedding from elongated rectangular cylinders at low Reynolds numbers 200-200^3 was investigated experimentally and numerically. The experiment was conducted in a low-speed wind tunnel, and the numerical analysis used the 2D Navier-Stokes equations and the finite difference method. In the experiment and in the numerical calculation, the side ratio of the rectangular cylinders evaluated ranged from 3 to 16 and from 3 to 10. The Strouhal number experiment and numerical analysis showed good agreement. It is generally known that the Karman vortex sheet, which forms when the two separated shear layers interact with one another behind the cylinder to create a staggered array of distinct vortices, characterizes the vortex shedding from short bluff cylinders like a circular and square-section cylinder. In contrast, our earlier research shown that a different sort of flow instability takes place when vortex shedding occurs from elongated bluff cylinders. It is here where a single separated shear layer may become unstable in the presence of a sharp downstream corner. This is what we refer to as the impinging shear-layer instability or more simply the edge tone. Wind tunnel measurements and numerical computations based on the finite-difference Navier-Stokes analysis were made on elongated rectangular cylinders at Reynolds numbers 20 & 103. The side ratio of the cylinders tested ranged from 3 to 16 in the experiment and 3 to 10 in the numerical analysis. **Murmu et al. (2020)** concerned this paper investigates the impact of turbulence intensity on the transport phenomena over two-dimensional bluff bodies. Both a square and an infinite circular cylinder with the same hydraulic diameter D—also the non-dimensional length scale—are simulated. The calculation is done for Reynolds numbers up to 200,000 and inlet turbulence intensities ranging from 5% to 40% to cover the cross flow enclosing the laminar and turbulent zone. The transition shear stress transport (SST) model for the closure of turbulence is solved along with the Reynolds-averaged Navier-Stokes and energy

equations. Initial experimental correlations and previous studies on drag and thermal performance are used to validate the results. **Murmu (2012)** investigated the flow and heat transfer studies over turbine blades have received considerably less attention in the literature than transport processes in external flows over bluff bodies, these studies do exist. Nevertheless, the flow field surrounding a turbine blade and related heat transfer vital for the machinery design of power plants. The design of a profile type blade is followed by modeling of the turbine blade with a Reynolds number range of 100 to 200 that includes both laminar and turbulent regimes. The governing equations of continuity, momentum equation, and energy have been solved for 50,000. Thus, it is clear that a single model may be applied successfully over the whole flow regime. The statistics also show that in a tumultuous environment, Nu's dependence on Re is stronger. Recall that a constant Nu is attained in internal flows quite frequently. However, in the stormy part, the value of Nu rises as a power of Re. It was discovered that Re till increased the average pressure coefficient and lift coefficient. **Murmu (2018)** performed the study of transport phenomena surrounding bluff bodies has garnered a lot of attention. The features of heat transfer inside a channel with a bluff body present and the impact of turbulence intensity on the transport process around a bluff body. A laminar and turbulent regime with Reynolds numbers between 10,000 and 200,000 as well as In this paper, turbulence intensities ranging from 5% to 40% are investigated. In this article, various bluff bodies are the subject of an operational research. The triangular prism, diamond, and trapezoidal bodies used as bluff bodies all have the same hydraulic diameter D, which also serves as the non-spatial length scale. the fluid being moved, Prandtl number (0.71) is considered to be constant for air. All flow regimes can be seamlessly connected using the SST Model to forecast heat transfer. The research measures how much inlet turbulence improves heat transfer from various bluff bodies. Investigated is how the severity of the turbulence affects the transport phenomena over two-dimensional bluff bodies. For the closure of turbulence, the transition SST Model is used to solve the governing equations for continuity, momentum, and energy. Experimental correlations validate the simulated results and demonstrate good agreement. In this work, it is shown that the transition SST Model can easily bridge all flow regimes for the heat transmission can be predicted. In this study, the impact of inlet turbulence intensity on improving the transfer of heat from the bluff bodies. The coefficients of drag and pressure are determined not be impacted by the size of the inlet turbulent flow. **Twardowski et al. (2016)** made a study on a combination of the many-body iterative T-matrix (MBIT) method and an enhanced application of the ray-by-ray (RBR) geometric optics method, the optical characteristics of diatom chains in the ocean are examined. The MBIT is a mechanism that provides precise numbers,favorably affecting scatterers with linear cells. Unlike other widespread geometric optics. The RBR, an approximation method, takes into account all rays' interference Comparing the two methodologies to benchmark simulations allows for their validation. With one or both procedures, results of diatom chains in a wide size range can be obtained,each of which is applicable to every optically soft particle, i.e., in the scenario where refractive index is getting close to one. The ray-tracing approach is used by the RBR method to determine the near field, and a volume integral equation. One cell is traced, and the outcome is

then applied to all other cells with reference to the periodic boundary conditions. Diatom chains' outcomes are displayed for many aspects diatom counts, ratios, sizes, incidence angles, and so on. To acquire the scattering characteristics for a wide variety of sizes, the RBR can be coupled. **Tiwari et al. (2014)** worked on the wake properties of unconfined flows over triangular prisms with various aspect ratios have been numerically analyzed. In order to do this, a fixed Cartesian-grid based numerical method using the porous media approach to replicate the effect of solid blocking has been made. Before the start of vortex shedding, the sub-critical regime to the super-critical regime have being thought of in this context within the confines of two-dimensionality. There have been suggested links between the wake bubble length and Reynolds number (Re) with different aspect ratios. When the tip of the triangular prism faces the approaching flow, linear dependency of the vortex bubble length on the Reynolds number has been found in the sub-critical zone. This behavior is pretty similar to that of circular cylinders.The prism steadily increases its aspect ratio. The power of the vortex has been blamed for this deteriorating nature generated behind the prism, which is then impacted by the fluid particles' slowing down as they go farther with severer cases of AR. The impact of aspect ratio on the crucial Reynolds number has now been discovered for both the arrangements. **Gandhi et al. (2016)** established an experimental investigation of the flow around a triangular prism and its relationship to apex angle. The goal of the study is to comprehend how the apex angle affects the flow structure and associated forces. At a Reynolds number of 520 (based on cylinder diameter), four triangular prisms are described with apex angles of 30, 45, 60, and 90 degree respectively. The hotwire and particle image velocimetry (PIV). Techniques for anemometry and flow visualization are utilized to describe the entire flow field. Results from the current study include the Strouhal number, drag coefficient, time-averaged results, as well as statistics such as the rms velocity, turbulence intensity, and shear stress, as well as the instantaneous velocity field. We see a linear relationship between the frequency of vortex shedding and the apex angle. The flow around a triangular prism is examined in this study along with the influence of the apex angle at Re = 520 (depending on cylinder diameter). The study's goal is to comprehend the impact of apex angle on the flow structure and associated forces. Strouhal number, drag coefficient, and other results are derived in the current work. Instantaneous and time-averaged velocity fields, statistics such as shear stress, rms velocity, and turbulence intensity for these apex angles compared. We are observing the apex angle and vortex shedding frequency. A greatest in Strouhal number and minimum in drag coefficient for apex angle 30 is observed. It corresponds to a narrow wake width from pictures of a flow visualization. **Chattopadhyay (2006)** has done the work on numerical investigation of heat transfer in a channel with a triangular prism has been conducted in the turbulent flow regime up to a Reynolds number of 40 000. The channel to prism element aspect ratio was set at 4.0. Using the SIMPLE technique, the Navier-Stokes equation and the energy equation have been solved, and the conventional k- formulation has been used for turbulence closure. The entry and exit regions were covered by a grid, and the region next to the prism element was discretized using an unstructured triangular mesh. According to the research, a triangular element increases heat transport in a channel by about 15%. Numerical simulation

was used to estimate the increase in heat transmission in a channel caused by the presence of a triangular element. About 15% of the order is enhanced. The enhancement is connected to increased skin friction, as would be predicted. The impact of the prism's aspect ratio the flow field and fluctuating density in a finite TP example are some of the crucial elements, which were not covered in the current work and will be in future works. **Bijjam (2020)** illustrated the flow of fluid and the transmission of heat across a long, equilateral triangular cylinder positioned in a horizontal channel are investigated in this study for Reynolds numbers up to 1e80 (in steps of 5) and Prandtl numbers up to 0.71 for a constant blockage ratio of 0.25. Using the commercial CFD solver FLUENT, the governing Navier-Stokes and energy equations, as well as the necessary boundary conditions, are resolved. A commercial grid generator called GAMBIT creates the computational grid. The fields of flow and temperature are shown, respectively, by the isotherm and streamline profiles. For the aforementioned range of conditions being researched, drag coefficient and average Nusselt number are computed here. It is discovered that the Reynolds number must be between and for the transition to a transient state to occur. For Reynolds number range 1-80 and Prandtl number 0.71, 2-D incompressible flow and heat transfer around a long, restricted, equilateral triangular cylinder have been explored in this study for a fixed 0.25 blockage ratio. The flow and temperature fields close to the triangular obstruction are each described by contours. The Reynolds number is discovered to have a value between Re =58 and Re =59. As the value increases, the mean drag coefficient lowers. Although the wake length rises with the Reynolds number for the variety of situations addressed here, Reynolds number.

2.1 Objective of the Thesis

After an extensive investigation of the literature on the turbulent promoters of investigations described above, the goal of this thesis has been set to address certain unresolved difficulties. These issues are what this study focuses on most:

a) To investigate flow phenomena around bluff bodies in various flow regimes with different inlet turbulence values.

b) To find out how channel walls become more effective and how heat is transferred around bluff bodies as a result of turbulence.

c) The variation of turbulent intensity with drag co-efficient and pressure co-efficient.

Chapter 3

METHODOLOGY

3.1 Introduction

With the help of various bluff shapes, this work investigates numerically how to improve heat transfer. This chapter provides a description of the process used to arrive at the solutions. It has been independently shown whether the flow is turbulent or laminar and therefore what flow regime it is. The flow structures that are produced during laminar, turbulent, as well as flow transitions between these two types of flow are analyzed in this case using a Reynolds-averaged Navier-Stokes equation (RANS)-based approach.

In this chapter, the process used to develop the solutions is described. The majority of the research reviewed in chapter 2 has independently proven which flow regime is present and whether the flow is turbulent or laminar. The flow structures that are created during laminar, turbulent, as well as flow transitions between these two types of flow, are investigated in this case using a Reynolds-averaged Navier-Stokes equation (RANS)-based methodology.

3.2 Transition Shear Stress Transport (SST) turbulence model

Depending on the time-averaged turbulence characteristics, turbulent flow predictions can be made. The process of time-averaging gives rise to fluctuating temperature and velocities in the conservation equations. In order to achieve this and make the Navier-Stokes equations tractable, the Reynolds Averaged Navier-Stokes (RANS) equations are used.

The momentum and energy equations are closed using a turbulent viscosity hypothesis that is framed within a RANS approach. The turbulent viscosity is obtained using the Transitional SST model of ("Menter et al. 2002"), allowing the simulation of all three flow regimes using a single formulation in an uninterrupted manner. The turbulence model requires the solution of the transport equations of three quantities, namely the turbulence kinetic energy (k), the specific dissipation rate (ω), the intermittency (γ) and the momentum thickness Reynolds number ($Re_{\theta t}$). Thus, with the three components of the momentum equation, the pressure correction equation (replacing the continuity equation) and the energy equation, the total number of field equations to be solved results in nine.

"Abraham et. al. (2009)" used transition SST model to predict the heat transfer characteristics in all flow regimes i.e., laminar, intermittent and turbulent. The authors used one set of Reynolds averaged conservation equations for mass, momentum and energy with two supplementary equations for turbulent viscosity and effective thermal conductivity and another set for turbulence containing equations to solve turbulent kinetic energy, specific rate of turbulence dissipation and intermittency. This irregularity can help in predicting the change from laminar to turbulent. The same Transition-SST model was used for predicting heat transfer in all flow regimes for various heat transfer problems effectively, namely parallel plate channels ("Minkowycz et. al. 2009"), Internal flows ("Abraham et. al., 2010 "and "Abraham et. al., 2011"), manufactured jets ("Abraham and Thomas 2009") and diverging conical ducts ("Sparrow et al. 2009"). As the pressure correction scheme, the SIMPLE scheme is used. For the discretization of the convective terms, the Second Order Upwind scheme is used for the momentum and energy equations, and the second Order Upwind scheme for the transport equations of the turbulence quantities. The convergence criteria for continuity, momentum and energy are set at 10^{-4}, 10^{-5} , and 10^{-7} respectively. The convergence criterion for the four turbulence quantities was also fixed at10^{-4} .

3.3 Governing equation

The three dimensional governing equations of continuity, momentum and energy equations are solved using transition SST model modified and proposed by "Abraham et. al. (2009)". The flow is steady, incompressible Ansys Fluent 16.0 is used to solve the following governing equations.

Continuity equation

$$\frac{\partial u_i}{\partial x_i} = 0 \qquad i=1, 2 \tag{3.1}$$

Momentum equation

$$\rho\left(u_i \frac{\partial u_j}{\partial x_i}\right) = -\frac{\partial p}{\partial x_i} + \frac{\partial}{\partial x_i}\left((\mu + \mu_{turb})\frac{\partial u_i}{\partial x_i}\right) \qquad j = 1,2 \tag{3.2}$$

Energy equation

$$\left(u_i \frac{\partial \Theta}{\partial x_i}\right) = \frac{\partial}{\partial x_i}\left(\left(\alpha + \frac{V_{turb}}{Pr_{turb}}\right)\frac{\partial \Theta}{\partial x_i}\right) \quad (3.3)$$

The values of turbulent Prandtl number (Pr_{turb}) are taken from ″Abraham et al. (2009)″. The laminar to turbulent modelling provided by the following equations for K and ω.

$$\frac{\partial(\rho u_i k)}{\partial x_i} = \gamma . P_k - \beta_1 \rho k \omega + \frac{\partial}{\partial x_i}\left(\left(\mu + \frac{\mu_{turb}}{\sigma_k}\right)\frac{\partial_k}{\partial x_i}\right) \quad (3.4)$$

$$\frac{\partial(\partial u_i \omega)}{\partial x_i} = A\rho S^2 - \beta_2 \rho \omega^2 + \left(\left(\mu + \frac{\mu_{turb}}{\sigma_\omega}\right)\frac{\partial_\omega}{\partial x_i}\right) + 2(1 - F_1)\rho \frac{1}{\sigma_{\omega 2}\omega}\frac{\partial_k}{\partial x_i}\frac{\partial_\omega}{\partial x_i} \quad (3.5)$$

Where $\mu_{turb} = \frac{a\rho k}{\max(a\omega, SF_{2)}}$ (3.6)

The working equations for the intermittency and intermittency adjunct function Π adopted [2002, 2009] are given below.

$$\frac{\partial(\rho\gamma)}{\partial_t} + \frac{\partial(\rho u_{i\gamma})}{\partial x_i} = P_{\gamma,1} - E_{\gamma,1} + P_{\gamma,2} - E_{\gamma,2} + \frac{\partial}{\partial x_i}\left(\left(\mu + \frac{\mu_{turb}}{\sigma_\gamma}\right)\frac{\partial \gamma}{\partial x_i}\right) \quad (3.7)$$

$$\frac{\partial(\rho\Pi)}{\partial_t} + \frac{\partial(\rho_{u_i}\Pi)}{\partial x_i} = P_{\Pi,t} + \frac{\partial}{\partial x_i}\left(\sigma_{\Pi,t}(\mu + \mu_{turb})\frac{\partial \Pi}{\partial x_i}\right) \quad (3.8)$$

The equations (3.4), (3.5), (3.7) and (3.8) are the additional equations which are solved along with regular equations of continuity (3.1), momentum (3.2) and energy (3.3) for calculating velocities, pressure, temperature, kinetic energy of turbulence, turbulence-specific dissipation, and intermittentness . The state of transition will depend on intermittency parameter (γ) which varies from 0 to 1. Near 0 value of γ determines the state as laminar, while the value near 1 determines the flow as turbulent. The term Π is again required for calculation of term F_1 in eqn. (3.5). The details are available in "Menter et al (2002)".

In equation (3.7) the transition sources are describe as follows:

$$P_{\gamma 1} = C_{a1} F_{len} \quad \rho S[\gamma F_{oneset}]^{c_{\gamma^3}} \tag{3.9}$$

$$E_{\gamma 1} = C_{a1} P_{\gamma 1} \gamma \tag{3.10}$$

Where S is the absolute value of shear strain rate, F_{length} is an empirical correlation which supervision the length of the transition zone, and C_{a1} and C_{e1} grasp the values of 2 and 1, accordingly. The desvastation /relaminarization sources are described as follows:

$$P_{\gamma 2} = C_{a2} \rho \Omega \gamma F_{turb} \tag{3.11}$$

$$E_{\gamma 2 = C_{e2}} P_{\gamma 2} \gamma \tag{3.12}$$

Where **Ω** is the vorticity magnitude. The transition onset is regulated by the following functions:

$$Re_v = \frac{\rho y^2 S}{\mu} \tag{3.13}$$

$$R_T = \frac{\rho k}{\mu \omega} \tag{3.14}$$

$$F_{oneset1} = \frac{Re_v}{2.193 Re_{\theta c}} \tag{3.15}$$

$$F_{oneset2} = min\big((F_{oneset1}, F^4_{oneset1}), 2.0\big) \tag{3.16}$$

$$F_{onese} = max\left(1 - \left(\frac{R_T}{2.5}\right)^3, 0\right) \tag{3.17}$$

$$F_{oeset} = max(F_{oneset2} - nF_{oneset3}, 0) \tag{3.18}$$

$$F_{turb} = e^{-\left(\frac{R_T}{4}\right)^4} \tag{3.19}$$

$Re_{\theta c}$ is the critical Reynolds number where the intermittency first starts to raise in the boundary layer. This happen upstream of the transition Reynolds number $Re_{\theta t}$ and the difference between the two must be achieve from an empirical correlation. Both the F_{leng} and $Re_{\theta c}$ interrelationship are tasks of $Re_{\theta t}$.

The constants for the intermittency equation are:

$C_{al} = 2;\ C_{e1} = 1;\ C_{a2} = 0.06;\ C_{e2} = 50;\ C_{\gamma 3} = 0.5;\ \sigma_{\gamma} = 1.0$

The governing equations along with appropriate closures were solved to obtain time-averaged flow and temperature fields, the governing equations and suitable closures were solved. It was decided to use the Patankar and Spalding (1972) solution procedure, which was implemented in Ansys Fluent 16.0. The following chapters go over the specifics of the solution process, including the choice of discretization schemes and convergence criterion.

The Nusselt number was calculated according to the following way,

$$N_u = \frac{hD_i}{K} \tag{3.20}$$

Where, k is the thermal conductivity of air and h is the convective heat transfer coefficient.

The Reynolds number based on hydraulic diameter of the object is given by,

$$\mathrm{Re} = \frac{\rho v D_i}{\mu} \tag{3.21}$$

It's necessary to understand the pressure and viscous forces affecting the bluff body in order to calculate the drag coefficients. The drag coefficient is obtained using this formula:

$$C_d = \frac{F_d}{\frac{1}{2}\rho {U_\infty}^2 A} \tag{3.22}$$

Where, F_d is the drag force acting on the bluff body.

The pressure co-efficient is defining as:

$$C_p = \frac{P - P_\infty}{\frac{1}{2}\rho {U_\infty}^2} \tag{3.23}$$

Where, p is the static pressureat the point at which pressure co-efficient is being evaluated,

p_∞ is the static pressure at free stream (i.e. remote from any disturbance)

ρ is the free stream fluid density and

U_∞ is the free stream velocity of the fluid.

Chapter 4

4.1 Computational domain

The first study investigates the forced convection cross flow around an octagonal bluff body. While an octagonal bluff body of side D which is also the hydraulic diameter. The non-dimensional distance between the inlet plane and the front surface of the octagonal bluff body is 15D and the non-dimensional distance between the rear surface of the octagonal bluff body and exit plane is 35D with the total non-dimensional length of the computational domain 50D. The ratio of one side of octagonal bluff body to the vertical distance between the upper and lower walls is, H=10D has been used in this work. The problem is considered to be two-dimensional and air is considered as working fluid.

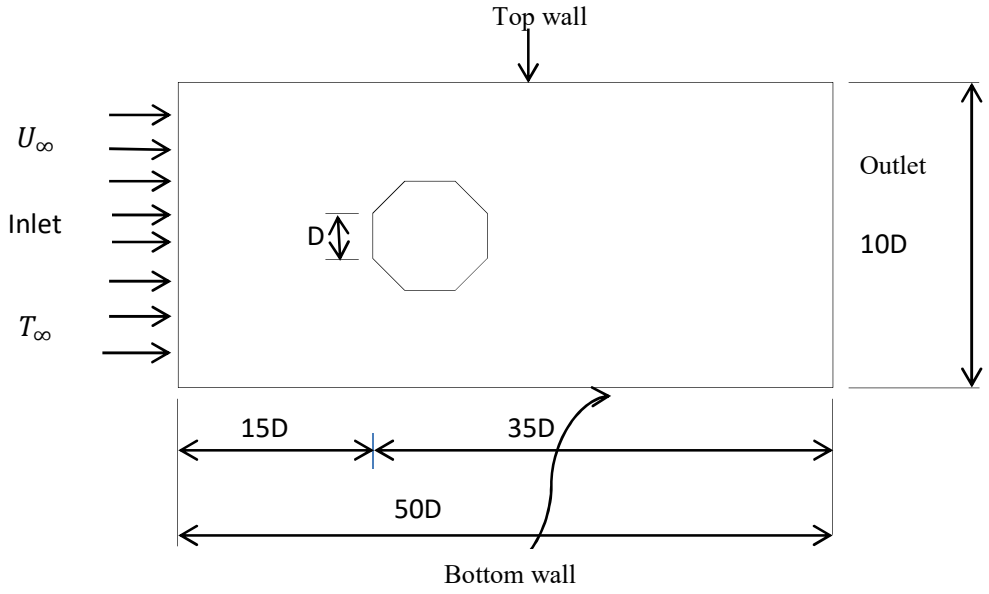

Fig.3: Computational domain

4.1.1 Boundary condition

The octagonal bluff body's constant surface temperature is kept at T_s=300 K as fluid with an inlet velocity of U_∞ and a temperature of T_∞ enters. Air is designated as the fluid, and its physical characteristics are constant (Pr=0.71), with an inlet temperature of 288 K. It is assumed that the top and bottom walls are symmetrical where the first derivative vanishes. Assuming that the fluid properties are constant and the domain size is fixed, the inlet velocity is changed to change the Reynolds number.

4.1.2 Solution Procedure

The Transient SST model, proposed by Abraham et al. (2009) used to solve the three-dimensional governing equations for continuity, momentum, and energy was discussed in Chapter 4**.** The governing equations were solved using ANSYSFLUENT 16.0, a commercial CFD program. The momentum equation was discretized by Leonard (1990) using the second order accurate QUICK scheme, and the energy equation was solved by Van Leer (1979) using the third order MUSCL.

When the scaled residual fell below a certain level, convergence of the solutions was assumed to have occurred 10^{-4} for momentum, 10^{-4} for continuity and 10^{-8} for energy equations. The gradients for temperature and were interpolated using a third-order accurate upwind scheme, whereas the gradients for intermittency (γ), turbulent kinetic energy, specific dissipation rate, and momentum thickness were done using a second-order accurate upwind scheme.

After performing rigorous check for grid independence, adequate numbers of cells were used. The number of nodes for the rectangular mesh are 50527 and the elements are 49913 used in this case. It was found that further refinement of grids do not lead appreciable change in results such as drag coefficient and Nusselt number distribution. In proceeding section, validation with experimental and available data from literature is also discussed. A part of the grid is shown in figure 4.

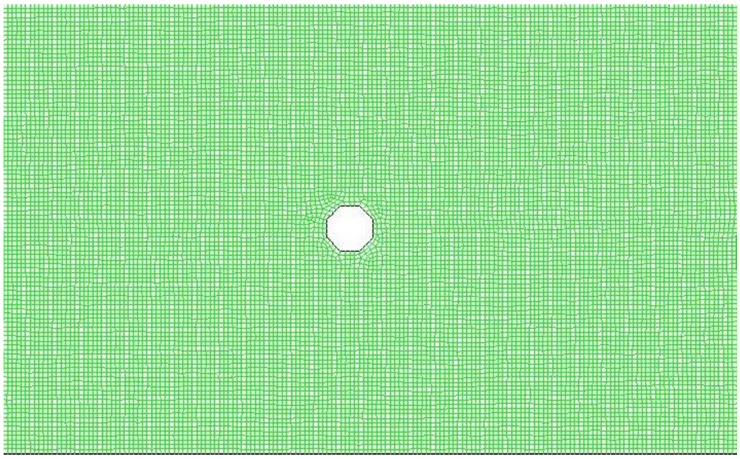

Fig. 4: Meshing geometry

Chapter 5

Results and Discussion

The simulation results that were obtained for various Reynolds numbers are covered in this section. Reynolds numbers up to 100,000 are used in the simulations. It is investigated how the average Nusselt number changes as the Reynolds number rises at a specific level of turbulence, and it is reported that the average Nusselt number increases as the intensity of the turbulence increases. The range of turbulence intensity is 5% to 40%.

5.1 Variation of Nu_{avg} with Re at different TI

In this section, results from a simulation with different Reynolds numbers and varying turbulence intensities are discussed. For Reynolds numbers ranging from 100 to 100,000, simulations are performed. The level of the turbulence intensity ranges from 5% to 40%. For the turbulence intensity levels of 5%, 10%, 20%, and 40% in the current work, an increase in Nusselt number has been noticed accompanied with an increase in Reynolds number. The graph below indicates that turbulence intensity has no effect on heat transfer rate for low Reynolds numbers, but that as the Reynolds number exceeds 10,000, the heat transfer coefficient significantly rises. The Nusselt number and the Reynolds number are approximately the same at 8,000.The Nusselt number, however, clearly rise with increasing turbulence intensity beyond this value of Re.

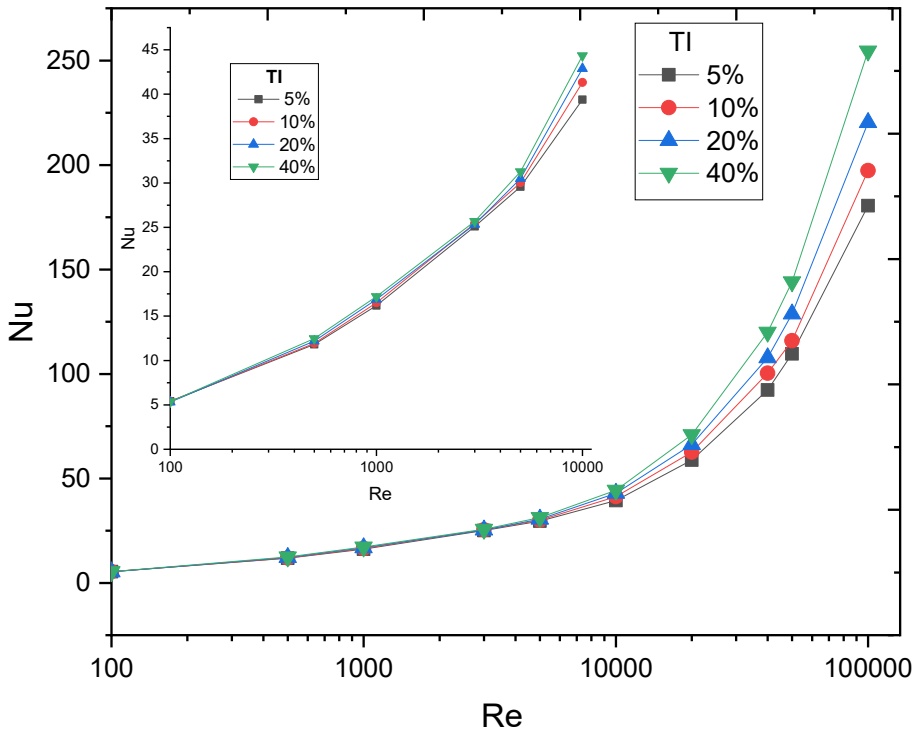

Fig. 5: Variation of Nu_{avg} with Re at different TI.

5.2 Variation of surface Nu with with different Re at fixed TI

The figure given below shows that the distribution of surface Nusselt number around the octagonal bluff body.While PABCDNEFGH is the surface of the octagonal bluff body.Since PABCDN and PHGFEN are symmetrically placed and showing similar distribution. From below figure it could be observed that there is a gradual rise in Nu in PA, steeply fall of Nu in AB while the flow is moving from B to C there is a sudden rise in Nu and it gradually drops while flow moves from C to N.As the flow reaches near E there is a rise in Nu and the same symmetrical behavior of Nu is observed for the symmetrical part PHGFEN of the octagonal bluff body.

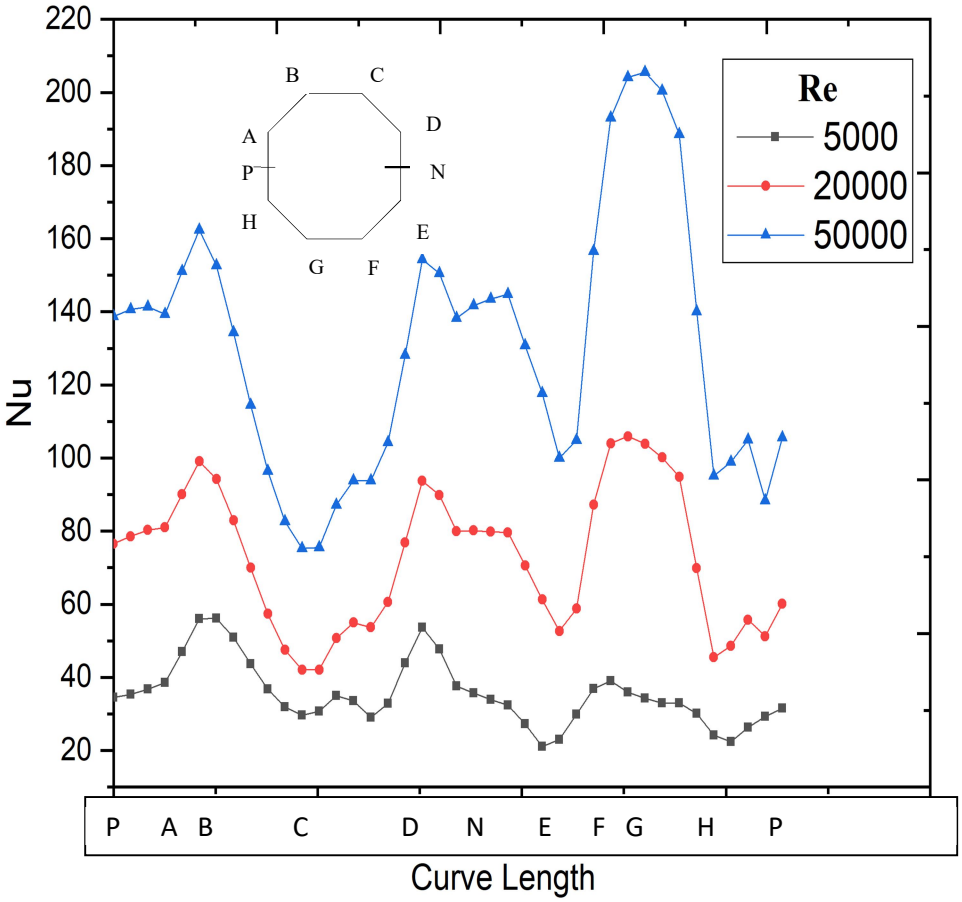

Fig. 6: Variation of surface Nu with different Re at fixed TI

5.3 Variation of surface Nu at different TI at Re=20,000

The figure 7, given below shows that the distribution of surface Nusselt number around the octagonal bluff body. While PABCDNEFGH is the surface of the octagonal bluff body. Since ABCDE and AHGFE are symmetrically placed and showing similar distribution. From below figure it could be observed that there is a gradual rise in Nu in AB, decreases in BC while the flow is moving from C to D there is a sudden rise in Nu and it gradually drops. Minimum Nu

(i.e.; almost equal to 100) at turbulent intensity 5% and maximum for 40% turbulent intensity while at zero curve length Nu for 20% and 40% are almost same. As the flow reaches near E again there is a rise in Nu and the same symmetrical behavior of Nu is observed for the symmetrical part AHGFE of the octagonal bluff body.

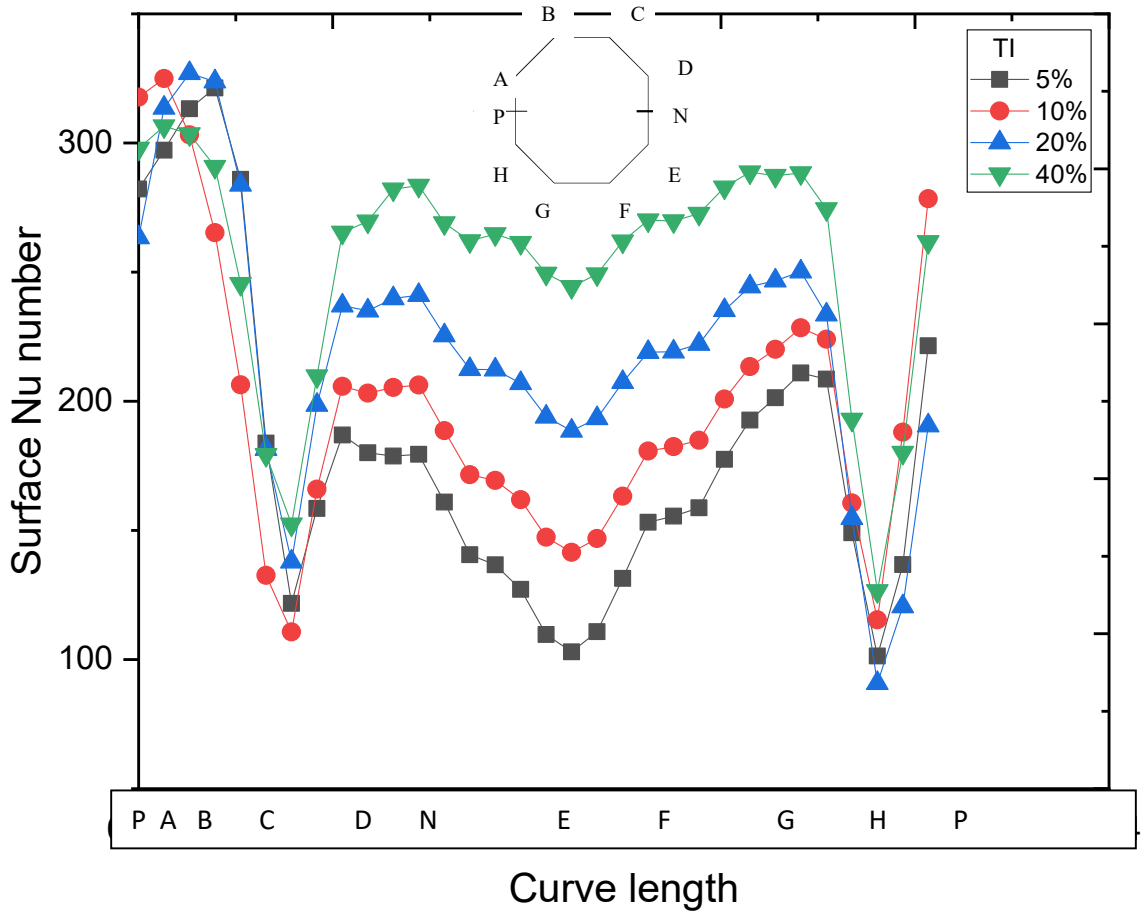

Fig.7: Variation of surface Nu at different TI at Re=20,000

5.4 Variation of pressure co-efficient with different Re

The pressure co-efficient (Cp) as seen in figure 8, shows a parabolic curve for flow over surface AB which a gradual symmetrical rise in Cp value from its minimum range around maximum magnitude of about 1.8 in the positive x-y plane. After reaching this maximum again decreases gradually. It has been observed that the Cp value pattern is similar while flow takes place over the surface PN and NP.

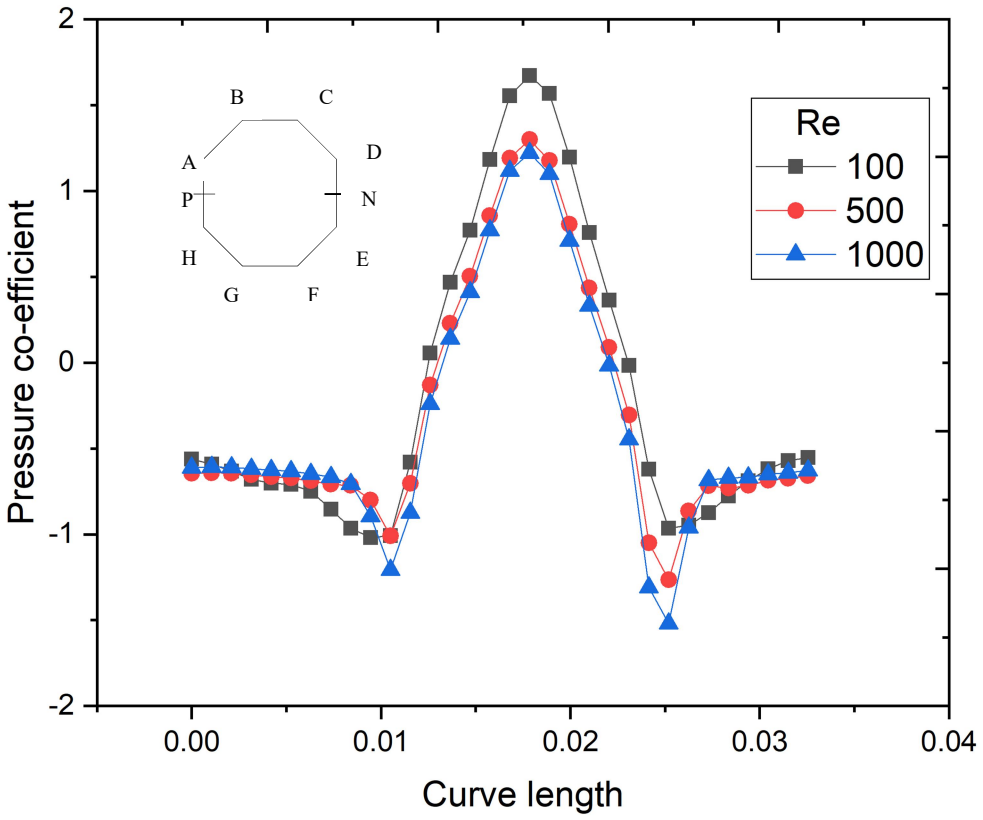

Fig. 8: Variation of pressure co-efficient with different Re

5.5 Variation of contours of stream function

Figure 9 below, stream functions at different Re is taken. There is little distinction between the contours, indicating that a stable thermal field has been established. A zone of substantially lower temperature is created in the wake of the octagonal bluff body. A cold circulation is seen at

the end of the bluff body. Stream functions for eight Reynolds number have been plotted. The low temperature core gets reduced in size as Re increases. The cold region moves front to rear of bluff body with increasing Reynolds number. The shape of the contour changes as the stagnation region moves to left with Reynolds number.

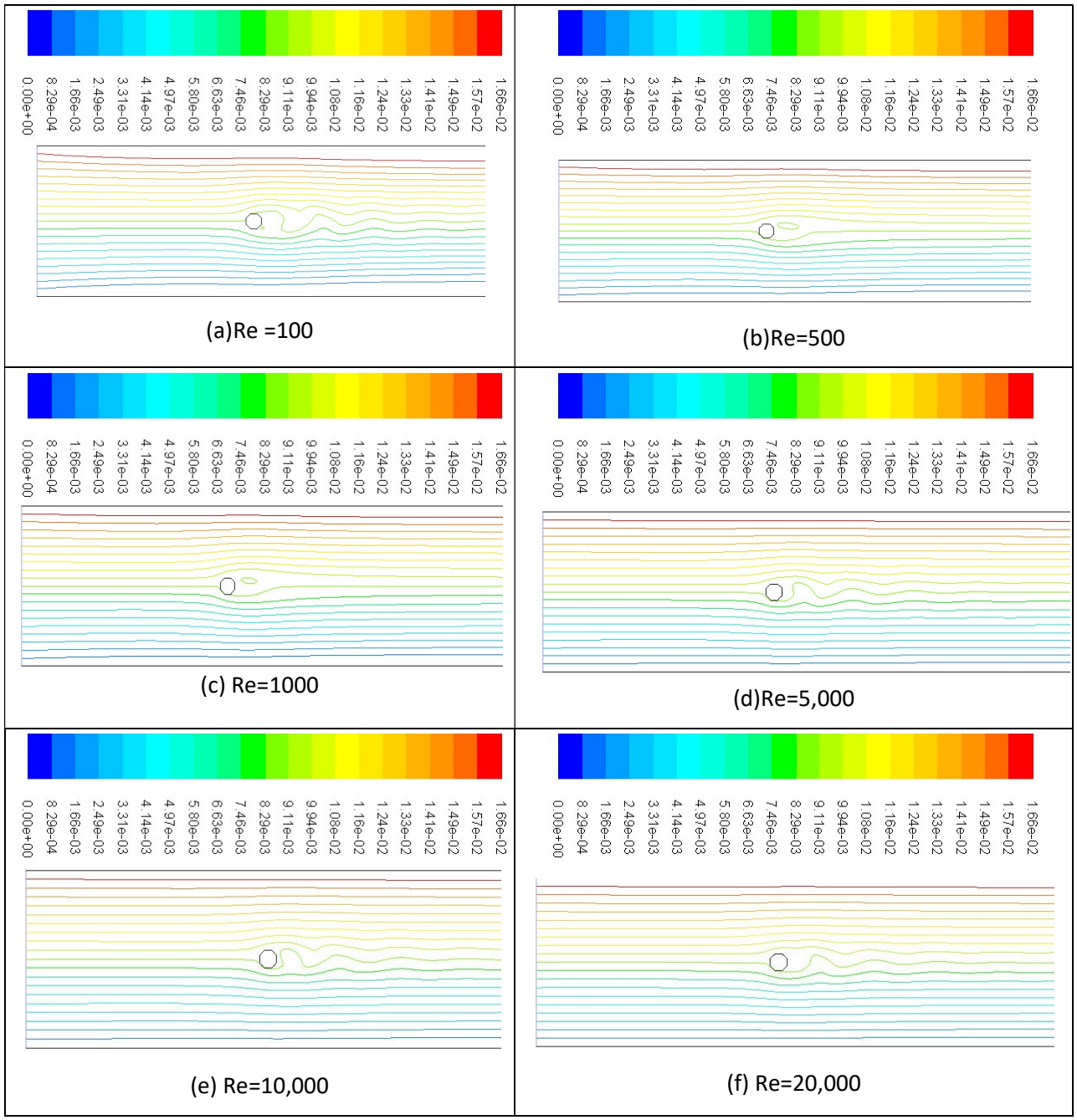

(a)Re =100

(b)Re=500

(c) Re=1000

(d)Re=5,000

(e) Re=10,000

(f) Re=20,000

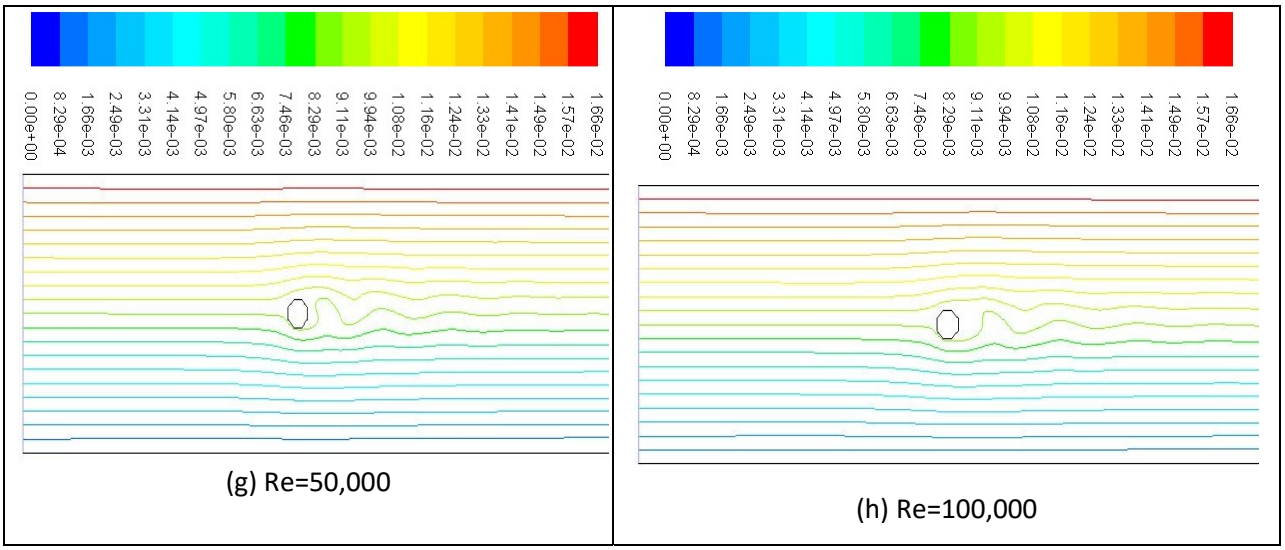

Fig. 9: Contours of stream function at (a) Re=100 (b) Re=500 (c) Re=1000 (d) Re=5000 (e)Re=10,000 (f)Re=20,000 (g)Re=50,000 (h)Re=100,000

5.6 Variation of temperature contours

Figure 10 shows below, temperature contours at six different R have been taken. It can be readily seen that a steady thermal filed has been established as no appreciable difference between the contours can be seen. In the wake of the bluff body relatively lower temperature zone is established. At the centre of the far bluff body cold circulation is noticed. Temperature contours for six different Reynolds number has been plotted. The low temperature core gets reduced in size as Re increases. The cold region moves to right with increasing Reynolds number. The shape of the contour changes as the stagnation region moves to left with Reynolds number.

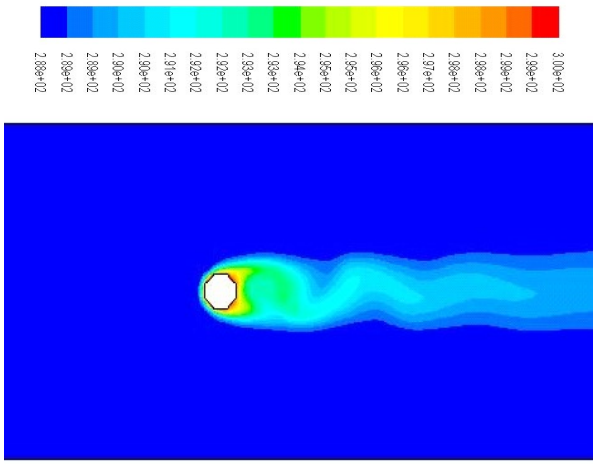

(a) Re=1,000

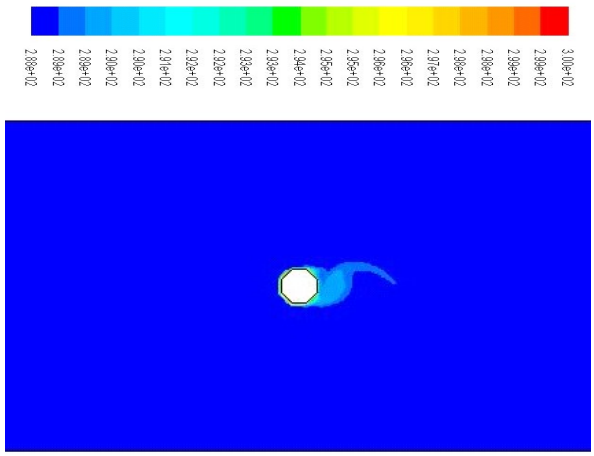

(b) Re=5,000

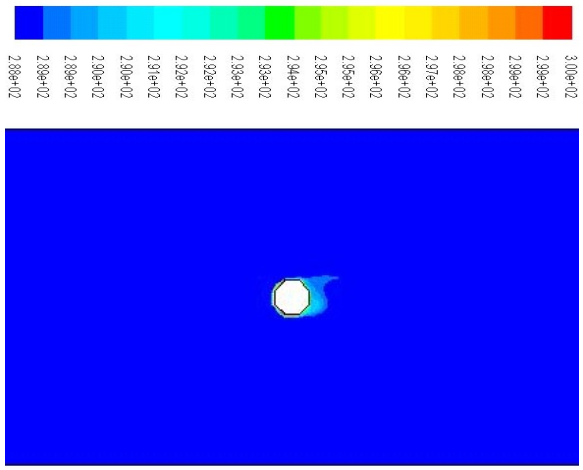

(c) Re=10,000

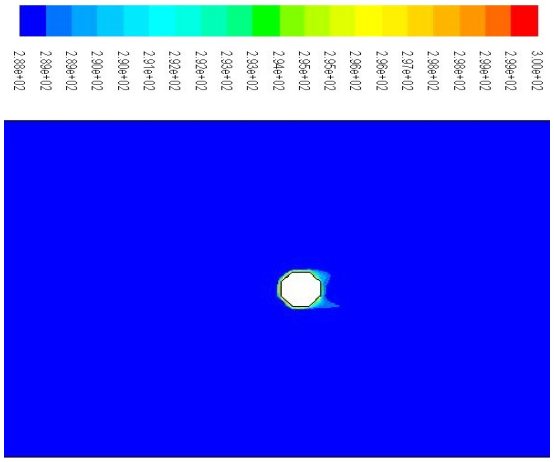

(d) Re=20,000

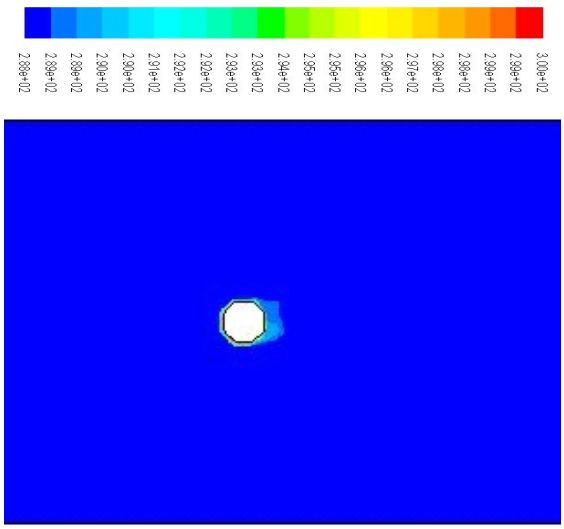

(e) Re=50,000

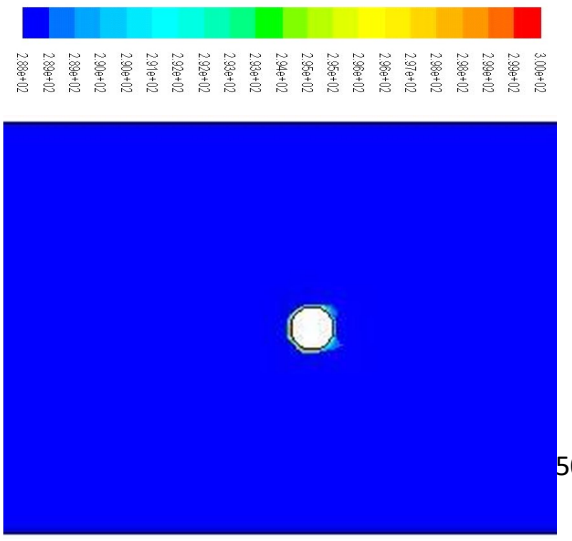

(f) Re=100,000

Fig. 10: Temperature contours at (a) Re=1000 (b) Re=5000 (c) Re=10,000 (d) Re=20,000 (e)Re=50,000 (f)Re=100,000

5.7 Variation of C_d with Re at different turbulent intensity.

Fig.11, shows the variation of C_d with different Re. It has been found that there is initially a sharp fall in C_d upto Re about 1000. Therafter there is gradual decrease of C_d value with increasing Re. It is also observed that there is an appreciable change of C_d varying TI.

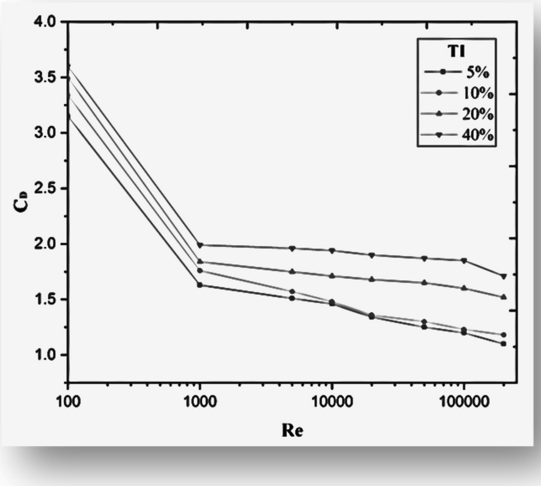

Fig.11:Variation of C_d with Re at different TI.

Chapter 6

Conclusions and Future scope

6.1 Conclusions

In this work, at first, a geometry of octagonal bluff body has been developed. After that, flow and heat transfer numerical evaluations were conducted. Through numerical simulation, the work makes predictions about the steady, two-dimensional incompressible flow and the thermal characteristics for a flow across an octagonal bluff body.

It has been found that:

1.The area weighted average of the Nusselt number is significantly affected by Reynolds number. As Reynolds number rises, it increases.

2. As the Reynolds number rises, the value of the pressure coefficient falls and monotonically.

3.The whole flow regime, including the laminar turbulent and transition regimes, may be predicted using the transition SST model. The results from the transition SST model and those from the purely laminar and turbulent models indicate quite well.

4. With the increase of Re Cd value decreases and with increasing TI Cd increases gradually.

6.2 Future Scope

The work is an initial attempt to study global transport phenomena around octagonal bluff body. The future works expected to have:

a) Three-dimensional analysis as we have only carried out studies in two dimensions.

b) Extend the work beyond Reynolds number 100,000.

(c) Extend work beyond the Prandtl number 0.71.

References

A. Prhashanna, Akhilesh K. Sahu, R.P. Chhabra, Flow of power-law fluids past an equilateral triangular cylinder: Momentum and heat transfer characteristics, International Journal of Thermal Sciences 50 (2011) pp.(2027-2041).

A. Richter, Petr A. Nikrityuk, Drag forces and heat transfer coefficients for spherical, cuboidal and ellipsoidal particles in cross flow at sub-critical Reynolds numbers, International Journal of Heat and Mass Transfer 55 (2012) pp.(1343–1354).

Afrrev Stech, 2D Flow around a Rectangular Cylinder: A Computational Study, Vol. 2 (1) January, 2013: pp. (1-26).

Amit Kumar Dhiman, Flow and Heat Transfer Phenomena around an Equilateral Triangular Bluff Body: Effect of Wall Confinement, Heat Transfer—Asian Research, 45 (7), 2016.

B.N. Rajani , A. Kandasamy, Sekhar Majumdar, Numerical simulation of laminar flow past a circular cylinder, Applied Mathematical Modelling 33 (2009) pp.(1228–1247).

Bingqiang Sun, George W. Kattawar , Ping Yang , Michael S. Twardowski , James M. Sullivan, Simulation of the scattering properties of a chain-forming triangular prism oceanic diatom, Journal of Quantitative Spectroscopy & Radiative Transfer 178 (2016) pp. (390–399).

Claudio Mannini, Ante Soda, Günter Schewe, Unsteady RANS modelling of flow past a rectangular cylinder: Investigation of Reynolds number effects, Computers & Fluids 39 (2010) pp. (1609–1624).

D. Yu, A. Kareem, Two-dimensional simulation of flow around rectangular prisms, Journal of Wind Engineering and Industrial Aerodynamics 62 (1996) pp.(131-161).

Dipankar Chatterjee and Bittagopal Monda, Forced convection heat transfer from an equilateral triangular cylinder at low Reynolds numbers, Heat Mass Transfer (2012) 48: pp. (1575–1587).

Fengming Wang, Jingzhou Zhang, Suofang Wang, Investigation on flow and heat transfer characteristics in rectangular channel with drop-shaped pin fins, Propulsion and Power Research (2012) pp. (64–70).

Fred L. Haan Jr., Ahsan Kareem and Albin A. Szewczyk, The effects of turbulence on the pressure distribution around a rectangular prism, Journal of Wind Engineering and Industrial Aerodynamics 77&78 (1998) pp. (381—392).

Himadri Chattopadhyay, Augmentation of heat transfer in a channel using a triangular prism, International Journal of Thermal Sciences 46 (2007) pp. (501–505).

https://images.app.goo.gl/vcZ77GZMkTnyPEYF9

Javad Taghinia, Md Mizanur Rahman and Timo Siikonen, Large eddy simulation of flow past a circular cylinder with a novel sub-grid scale model, European Journal of Mechanics B/Fluids 52 (2015) pp.(11–18).

Ju Y. You and Oh J. Kwon, Numerical assessment of turbulent models at a critical regime on unstructured meshes, Journal of Mechanical Science and Technology 26 (5) (2012) pp.(1363~1369).

Ki-Deok Ro, Experimental characterization of flow field around a square prism with a small triangular prism, Journal of Mechanical Science and Technology 29 (4) (2015) pp. (1649~1656).

M. Belloli , F. Fossatia , S. Giappino , S. Muggiasca and F. Robustelli , Turbulence intensity effect on the bluff bodies aerodynamic behavior, The Seventh International Colloquium on Bluff Body Aerodynamics and Applications Shanghai, China; September 2-6, 2012.

M. Mallick and A. Kumar, Study on Drag Coefficient for the Flow Past a Cylinder, International Journal of Civil Engineering Research 5 (2014) pp.(301-306).

M. Ozgoren, Flow structure in the downstream of square and circular cylinders, Flow Measurement and Instrumentation 17 (2006) pp.(225–235).

M. Saeedi, P. P. LePoudre, Bing-Chen Wang, Direct numerical simulation of turbulent wake behind a surface-mounted square cylinder, Journal of Fluids and Structures 51 (2014) pp.(20-39).

M.R. Ruith, P. Chen and E. Meiburg, Development of boundary conditions for direct numerical simulations of three-dimensional vortex breakdown phenomena in semi-infinite domains, Computers & Fluids 33 (2004) pp. (1225–1250).

Muk Chen Ong, Torbjorn Utnes, Lars Erik Holmedal, Dag Myrhaug and Bjørnar Pettersen, Numerical simulation of flow around a smooth circular cylinder at very high Reynolds numbers, Marine Structures 22 (2009) pp. (142-153).

Namit Agrwal, Sushanta Dutta, B.K. Gandhi, Experimental investigation of flow field behind triangular prisms at intermediate Reynolds number with different apex angles, Experimental Thermal and Fluid Science 72 (2016) (97–111).

O. Zeitoun, Mohamed Ali, A. Nuhait, Convective heat transfer around a triangular cylinder in an air cross flow, International Journal of Thermal Sciences 50 (2011) pp. (1685-1697).

Pietro Catalano, Meng Wang, Gianluca Iaccarino and Parviz Moin, Numerical simulation of the flow around a circular cylinder at high Reynolds numbers, International Journal of Heat and Fluid Flow 24 (2003) pp. (463–469).

R.M. Stringer, J. Zang, A.J. Hillis, Unsteady RANS computations of flow around a circular cylinder for a wide range of Reynolds numbers, Ocean Engineering 87 (2014) pp. (1–9).

Ravi Golani1 and A. K. Dhiman, Fluid flow and heat transfer across a circular cylinder in the unsteady flow regime, The International Journal of Engineering and Science (IJES), Volume 3, (2014) pp. (08-19).

Richa Agarwal and Amit Dhiman, Time-periodic non-Newtonian power-law flow across a triangular prism, J Braz. Soc. Mech. Sci. Eng. (2016) 38: pp. (227–240).

S. C. Murmu and H. Chattopadhyay, Effect of inlet turbulence intensity on transport phenomena over bluff bodies, Volume 47, Issue 6, 2020, pp. (485-499).

S. C. Murmu, Flow and heat transfer around a turbine blade, (2012), pp. (1-71).

S. Ganga Prasath, M. Sudharsan, V. Vinodh Kumar, S.V. Diwakar , T. Sundararajan , Shaligram Tiwari , Effects of aspect ratio and orientation on the wake characteristics of low Reynolds number flow over a triangular prism, Journal of Fluids and Structures 46 (2014) pp. (59–76).

S. Oka , T. Ishihara, Numerical study of aerodynamic characteristics of a square prism in a uniform flow, J. Wind Eng. Ind. Aerodyn. 97 (2009) pp.(548–559).

S. Srikanth, A.K. Dhiman, S. Bijjam, Confined flow and heat transfer across a triangular cylinder in a channel, International Journal of Thermal Sciences 49 (2010) pp. (2191-2200).

Shams-Ul-Islam, Waqas Sarwar Abbasi, Hamid Rahman, Force Statistics and Wake Structure Mechanism of Flow around a Square Cylinder at Low Reynolds Numbers, International Journal of Mechanical, Aerospace, Industrial, Mechatronic and Manufacturing Engineering Vol:8, (2014) pp.(1405-1411).

Sridhar Ravi, Simon Watkins, Jon Watmuff, Phred Petersen and Matthew Marino, The influence of turbulence intensity on the flow structure over a thin airfoil at low Reynolds numbers, 28th international congress of the aeronautical sciences.

Sudhir Chandra Murmu, Some studies on some studies on studies on transport transport phenomena in presence of a bluff body, 2018 pp. (1-148).

Toukir Islam and S.M. Rakibul Hassan, Experimental and Numerical Investigation of Flow over a Cylinder at Reynolds Number 10^5, Journal of Modern Science and Technology Vol. 1. May (2013) pp. (52-60).

W.J. Minkowycz, J.P. Abraham, E.M. Sparrow, Numerical simulation of laminar breakdown and subsequent intermittent and turbulent flow in parallel-plate channels: Effects of inlet velocity profile and turbulence intensity, International Journal of Heat and Mass Transfer 52 (2009) pp.(4040–4046).

Y. Nakamuraa, Y. Ohya, S. Ozono, R. Nakayamaha, Experimental and numerical analysis of vortex shedding from elongated rectangular cylinders at low Reynolds numbers 200-100^3, Journal of Wind Engineering and Industrial Aerodynamics 65 (1996) pp. (301~308).

Y. Srinivas, G. Biswas, A. S. Parihar and R. Ranjan, Large-Eddy Simulation of High Reynolds Number Turbulent Flow Past a Square Cylinder, Journal of engineering mechanics, march 2006.

Z. Zhu, H. Yang, T. Chen, Numerical study of turbulent heat and fluid flow in a straight square duct at higher Reynolds numbers, International Journal of Heat and Mass Transfer 53 (2010) pp.(356–364).